Gravitational Forces Between Nonclassical Mechanical Oscillators

Yulong Liu,[1,2] Jay Mummery,[3] Jingwei Zhou,[2] and Mika A. Sillanpää[2,*]

[1]*Beijing Academy of Quantum Information Sciences, Beijing 100193, China*

[2]*Department of Applied Physics, Aalto University, P.O. Box 15100, Aalto FI-00076, Finland*

[3]*ARC Centre of Excellence for Engineered Quantum Systems, University of Western Australia,
35 Stirling Highway, Crawley WA 6009, Australia*

Interfacing quantum mechanics and gravity is one of the great open questions in natural science. Micromechanical oscillators have been suggested as a plausible platform to carry out these experiments. We present an experimental design aiming at these goals, inspired by Schmöle *et al.* [Class. Quantum Grav. 33, 125031 (2016)]. Gold spheres weighing of the order of a milligram will be positioned on large silicon nitride membranes, which are spaced at submillimeter distances from each other. These mass-loaded membranes are mechanical oscillators that vibrate at about 2 kHz frequencies in a drum mode. They are operated and measured by coupling to microwave cavities. First, we show that it is possible to measure the gravitational force between the oscillators at deep cryogenic temperatures, where thermal mechanical noise is strongly suppressed. We investigate the measurement of gravity when the positions of the gravitating masses exhibit significant quantum fluctuations, including preparation of the massive oscillators in the ground state, or in a squeezed state. We also present a plausible scheme to realize an experiment where the two oscillators are prepared in a two-mode squeezed motional quantum state that exhibits nonlocal quantum correlations and gravity at the same time. Although the gravity is classical, the experiment will pave the way for testing true quantum gravity in related experimental arrangements. In a proof-of-principle experiment, we operate a 1.7 mm diameter Si_3N_4 membrane loaded by a 1.3 mg gold sphere. At a temperature of 10 mK, we observe the drum mode with a quality factor above half a million at 1.7 kHz, showing strong promise for the experiments. Following implementation of vibration isolation, cryogenic positioning, and phase noise filtering, we foresee that realizing the experiments is in reach by combining known pieces of current technology.

I. INTRODUCTION

It was not until the 1930s that it became legitimate to ask whether quantum-mechanics, which holds for elementary particles, could also be used to describe degrees of freedom in larger bodies [1]. Such "secondary" macroscopic quantum phenomena are distinguished from, for example, magnetism or many other properties of solid matter that are of a very quantum origin. In contemporary experimental research, secondary macroscopic quantum-mechanical phenomena, for example, superpositions, entanglement, energy quantization, and zero-point noise, are routinely observed with large molecules [2], atomic ensembles [3], superconducting microcircuits [4], or, in particular, in the motion of micromechanical oscillators; see, e.g., Ref. [5]. As compared to normal atomic quantum phenomena, it is much more challenging to create and observe macroscopic quantum effects since they are more fragile with respect to environmental decoherence.

The theory of general relativity, in the same way as quantum mechanics in its own realm, has been extraordinarily successful in describing huge objects interacting via gravitational force. One of the greatest results predicted by general relativity was the discovery of gravitational waves by the Laser Interferometer Gravitational-Wave Observatory (LIGO) detector [6]. Regrettably, general relativity and quantum mechanics do not get along well at all. For example, time in quantum mechanics is an absolute quantity, whereas in relativity it is a dynamic variable. The theory resulting from blindly quantizing general relativity is not renormalizable and hence far from satisfactory at a fundamental level. It is not even known if gravity is a quantum-mechanical entity whatsoever, or whether it is somehow disconnected from the rest of the universe that obeys quantum mechanics. One can say that the main point in the studies is to find out if the gravitational field created by a quantum superposition state is a quantum superposition of the two fields.

On the experimental side, the situation is equally bleak. Quantum gravity, if such an entity exists, plays a role at

_____

*mika.sillanpaa@aalto.fi

the respective Planck length, time, or energy scales of approximately 10^{-35} m, 10^{-44} s, and 10^{19} GeV. Direct experimental access to these extraordinary scales is not possible in the foreseeable future.

Interestingly, it has been realized recently that indirect measurements could probe the gravity-quantum interface. Oscillating physical bodies in the motional quantum regime—vaguely speaking with a thermally excited phonon number less than one—might be well suited for the purpose [7–12]. Since 2010 [5], nonclassical motional states are quite routinely achieved in various types of nano- and micromechanical oscillators in the size range up to approximately 10 μm, weighing up to a nanogram. In many experiments, a setup known as cavity optomechanics has been utilized, where mechanical oscillations are coupled to electromagnetic fields located inside cavity resonators of various geometries and frequencies [13]. A benchmark would be to prepare a quantum state in an oscillator whose mass exceeds the mass equivalent of about 20 μg of the Planck energy, which represents a plausible crossover above which quantum states have been hypothesized to decohere [14,15]. Experimental preparations have been going on to cool oscillators with these heavy effective masses towards the motional ground state [16–21]. Microwave cavity optomechanics [22] offers another possibility as a side product from the more complex scheme we discuss below.

Putting aside quantum gravity for a moment, measuring the effect of Earth's gravity on a small quantum object is an interesting goal, achieved with neutron interferometry since the 1970s [23,24], and followed by experiments on cold atoms [25,26]. The next and more demanding step is arguably verifying the gravitational force between very small objects. Being able to make such a measurement is likely a prerequisite for more delicate measurements that involve both gravity and quantum phenomena inside the system. Since the Cavendish experiment at the end of the eighteenth century, the masses between which gravitational forces have been directly measured have got smaller [27], reaching subgram source masses [28,29] at a distance of about 200 μm. Even lower source masses consisting of a 0.2 gram hole have been claimed [30]. The aim in these torsion balance experiments and in many earlier [31–34] has been to test deviations from Newton's law of gravity at very small distances, although typically they have been null measurements without directly measuring the gravity.

It has been proposed that micromechanical devices could push the mass limit of detecting a purely Newtonian gravitational force down to the milligram range of source masses [35]. Very recently, the scheme was experimentally demonstrated [36]. According to the scheme, the source mass is strongly actuated. The time-dependent gravitational pull can be sensed by taking advantage of resonant enhancement, where the test mass is sitting on a vibrating beam. In the current paper we describe a concrete
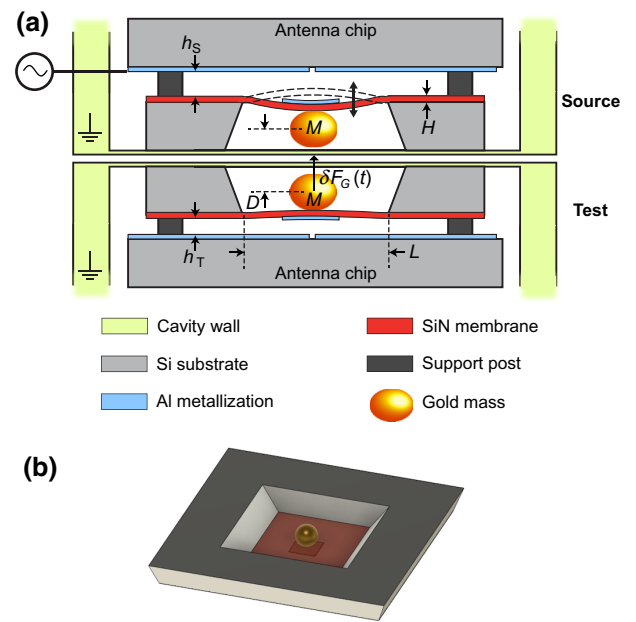

FIG. 1. Schematics of the proposed experiment. (a) Side view of two flip-chip assemblies with mass-loaded high-stress silicon nitride membranes, which are positioned at a submillimeter distance from one another. There can be an appreciable gravitational force between the gold spheres, which can be observed using microwave optomechanical techniques, for which the metallized antennas mediate coupling. (b) Rendering of one mass-loaded membrane chip.

proposal that can realize, first of all, the measurement of self-gravity in a system of milligram particles. As compared to Schmöle *et al.* [35], who considered room-temperature operation and frequencies less than 100 Hz, our scheme aims at higher frequencies of several kilohertz and deep cryogenic temperatures in order to reach the quantum regime.

A sketch of the device scheme is shown in Fig. 1. We utilize microwave cavity optomechanics that is naturally compatible with cryogenics, which also offers the benefit of reduced dissipation. The main interest is on finding a way to determine gravity when the source mass or the test mass, or both, are localized at the vacuum level and thus exhibit significant vacuum fluctuations. The possible experiment will not yet create superposed gravitational fields because the positions of the masses are not in any appreciably spatially separated superposition. In our view, however, this detailed proposal is unique in the sense that its implementation seems readily in reach to touch the interface between quantum mechanics and gravity, and it would present an important step on this very fundamental line of research.

II. THEORY AND MODELING

In this section, we discuss various aspects on the underlying theory, and present results of numerical modeling

and compare these against achievable experimental parameters.

A decisive prerequisite for these sensitive measurements will be the elimination of thermal noise of the mechanical mode. In thermal equilibrium, an oscillator of a resonance frequency ω_0 has the thermally excited phonon number $n_m^T = [\exp(\hbar\omega_0/k_B T) - 1]^{-1}$. Low-order flexural mechanical modes in whatever system tend to be of a much lower frequency than, say, electromagnetic modes, and therefore usually $n_m^T \gg 1$ even at deep cryogenic temperatures. Thus, reaching the pertaining quantum regime in mechanical systems in general is challenging. However, reaching this limit using various cooling techniques in cavity optomechanics is these days quite standard. The basic requirement is that the phonon number $n_m \ll n_m^T$ associated with a remaining thermal population is of the order of 1, or better, much less than 1.

A. Microwave cavity optomechanics

Traditionally, cavity optomechanics has studied the interaction between a mechanically vibrating mirror with the light field inside an optical Fabry-Pérot resonator. The coupling between light and motion is due to radiation pressure. The important parameters include the single-photon radiation-pressure coupling energy g_0, the mechanical resonance frequency ω_0, the intrinsic mechanical damping rate γ_0, and the quality factor Q, as well as the resonance frequency ω_c and the damping rate κ of the cavity. The latter is further split into internal and external losses: $\kappa = \kappa_{\text{int}} + \kappa_{\text{ext}}$. The Hamiltonian becomes

$$H = \omega_c a^\dagger a + \omega_0 b^\dagger b + g_0 a^\dagger a(b + b^\dagger), \quad (1)$$

where the creation and annihilation operators for photons (phonons) are denoted by a, $a^\dagger$ (b, $b^\dagger$).

Complicated quantum state control can be achieved via combinations of the basic operations created by applying coherent electromagnetic waves at frequencies corresponding to Stokes or anti-Stokes motional sidebands of the cavity. Although the g_0 parameter is small compared to other scales, the pumping tones can also be seen as creating a large effective coupling $\mathcal{G} = g_0\sqrt{n_P}$, where $n_P \gg 1$ is the pump-induced photon number. Nearly arbitrary (Gaussian) quantum operations can be performed by suitable pumping with many coherent tones. The scheme is easily extended to multipartite systems. A carefully designed pumping can also be seen to turn the cavity into a dissipative reservoir such that the oscillator sees a dissipative bath that pulls the oscillator into a nontrivial steady state.

Some of the important experimental advances in the field of quantum cavity optomechanics include sideband cooling to the ground state [37,38], entanglement between microwave light and motion [39], radiation-pressure shot noise and optomechanical squeezing [40–44], non-Gaussian mechanical states [45], motional entanglement

between mechanical oscillators [46,47], the Bell test [48], and room-temperature quantum behavior [49,50].

The basic method to cool down mechanical oscillators in cavity optomechanics at large is sideband cooling. The coherent pump tone is applied at a frequency that is one ω_0 lower than the cavity frequency. Then, phonons are preferentially scattered into the cavity. In order for this protocol to work well, the good-cavity (resolved-sideband) limit $\kappa \ll \omega_0$ has to be satisfied. The oscillator acquires an optical damping $\Gamma_{\text{opt}} = 4\mathcal{G}^2/\kappa$, such that its linewidth is broadened up to

$$\gamma = \gamma_0 + \Gamma_{\text{opt}}. \quad (2)$$

Including a bad-cavity correction [the last term in Eq. (3) below], the final thermal phonon occupation of the mode is given by

$$n_m = n_m^T \frac{\gamma_0}{\gamma} + \left(\frac{\kappa}{4\omega_0}\right)^2. \quad (3)$$

Microwave-frequency "cavities" are one of the leading platforms to do cavity optomechanics in the wide sense. Usually, these have been realized as on-chip superconducting transmission line resonators. An overwhelming benefit of the microwave-frequency realization is its compatibility with standard cryogenic instrumentation. The mechanical resonators in this setup have usually been either nanowires [22,51–53] or aluminum drumheads [37,46,54–56]. A very promising recent advance has been achieved with high-stress silicon nitride membranes of several hundred microns in diameter that were implemented inside three-dimensional (3D) microwave cavities [57,58], which is the setup we are interested in.

The analog of radiation-pressure coupling arises through the fact that a conducting mechanical oscillator modulates the cavity capacitance. Usually, the capacitor is an approximate plate capacitor defined by a membrane oscillator and a counter electrode that is connected to the cavity. For example, in Fig. 1(a), there are two such movable capacitors, with the vacuum gaps denoted as h_S and h_T.

The single-quantum radiation-pressure coupling, here given in frequency units, becomes

$$g_0 \equiv \frac{d\omega_c}{dx} x_{\text{ZP}} = \frac{\omega_c}{2C}\left(\frac{dC}{dx}\right)x_{\text{ZP}}, \quad (4)$$

where C is the total capacitance of the LC cavity resonator and $x_{\text{ZP}} = \sqrt{\hbar/2M\omega_0}$ is the mechanical zero-point oscillation amplitude, with M the effective mass.

If we suppose that the empty cavity's capacitance dominates over the movable one, we can write Eq. (4) as

$$g_0 \simeq \frac{\omega_c}{2C}\left(\frac{\varepsilon_0 A}{h^2}\right)x_{\text{ZP}}, \quad (5)$$

where A is the electrodes' surface area and h is the vacuum gap. This shows that a narrow vacuum gap is a critical parameter for maximizing the coupling.

B. Mass-loaded membrane

We select stoichiometric, high-stress Si_3N_4 (hereafter SiN) as the membrane material due to its well-known excellent mechanical properties, and suitability for (microwave) cavity optomechanics [57,58]. The internal materials loss is shunted by the high prestress, and very high $Q \sim 10^9$ at a megahertz frequency can be reached even at elevated temperatures [44,59,60]. Let us consider a rectangular SiN membrane with side length L, thickness H, density $\rho \simeq 3.2 \times 10^3$ kg/m^3, and prestress $\sigma \simeq 900$ MPa. Without any mass loading, the lowest drum mode has frequency $\omega_0/2\pi \simeq (0.71/L)\sqrt{\sigma/\rho}$. For example, with $L = 5$ mm, $\omega_0/2\pi \simeq 76$ kHz.

Let us now add the mass loading. A natural material choice is gold due to its high density and well-characterized properties. A spherical mass M with radius R is glued in the center of the membrane. The glue is modeled as a short cylinder of radius $r_{glue} < R$. Because of the added mass overwhelming the membrane mass, the mode frequency will substantially decrease. We are not aware of an expression for the frequency of a loaded rectangular membrane. We adapt the corresponding result for the circular eardrum [61]:

$$f_0 = \omega_0/2\pi \approx \sqrt{\frac{\sigma H}{2\pi M \log(L/2r_{glue})}}. \qquad (6)$$

The frequency depends now on the membrane thickness, but not directly on its width. However, the frequency depends significantly on the participation ratio of the glue spot, and goes down when the spot size decreases. The latter is because the less contact area there is between the mass and the membrane, the less tensile force will pull the mass.

We ran finite-element model (FEM) simulations to verify the mode profiles. For the simulation, the glue is modeled as a cylinder connecting the membrane and the sphere. An example mode shape is shown in Fig. 2. In a couple of tests using different parameter values, Eq. (6) holds to within 10%. In addition to the main flexural mode, there are two ideally degenerate modes where the sphere wobbles horizontally. Their frequency depends sensitively on the glue spot size, and is typically lower than that of the main mode. There are no other modes within a decade in frequency of the main mode. One can easily verify from the simulations that the weight of the sphere does not significantly deflect the membrane in comparison to a typical vacuum gap, neither does it affect the mode profiles almost independently of the orientation of the chip with respect
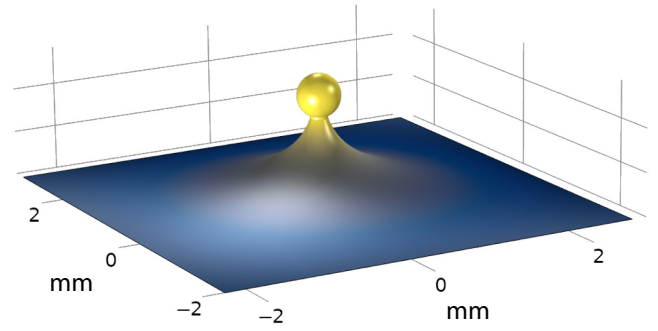

FIG. 2.   Mass-loaded drum mode. The finite-element simulation shows the profile of the lowest drum mode of an $L = 5$ mm wide, $H = 100$ nm thick rectangular silicon nitride membrane with an $R = 0.25$ mm radius gold sphere glued in the center. The glue spot radius is $r_{glue} = 100$ μm. The mode frequency becomes $f_0 \simeq 1.9$ kHz.

to the horizontal. These are due to the high tension in the membrane.

With the high mass load, the optomechanical coupling, Eq. (4), will be reduced because the zero-point motion will go down, while the electrode geometry can be assumed unchanged. The dependence of g_0 on the mass load is only weak, $g_0 \propto M^{-1/4}$. Using the discussed parameters, g_0 amounts to about 30% of that of a bare membrane. With a 0.5 μm vacuum gap between the electrodes, we have $g_0/2\pi \sim 0.2$ Hz, which is still a very decent value as will be discussed below in light of other experimental parameters.

A critical consideration is how the mechanical losses are influenced by the exceptional geometry. It can be expected that especially the glue, but also the gold, can have high losses even at cryogenic temperatures. As seen in Fig. 2, the mode profile exhibits a sharp kink at the joint between the membrane and the glue. A large curvature is known to enhance the losses of the mode [59,62]. In the FEM simulation we take care that the mesh around the kinks is small (0.5 μm) in comparison to the resulting bending radius (about 3 μm). For SiN, we use a low-temperature loss factor of about 10^{-5}. Using the parameters mentioned in Fig. 2, we find that SiN losses set $Q \lesssim 2 \times 10^8$. Although curvature is strongly enhanced at the kink, it is at the same time decreased in the regions away from the center. This could also reduce the losses due to clamping, although this is not considered in the simulations.

For gold or epoxy, the low-temperature loss is not readily available. For the epoxy, we use that of PMMA, of the order of about 10^{-3} [63], and assume the same for gold. Including all the estimated losses, the total Q value is obtained from $Q^{-1} = \sum Q_i^{-1}$, summing all the considered loss channels i. In the current example, $Q \sim 7 \times 10^6$ for the main mode, strongly dominated by losses of the glue. The contributions by different loss channels are listed in

TABLE I.　Mechanical Q values due to material losses. The last column gives the total Q with the parameters $\eta_{\mathrm{SiN}} = 10^{-5}$, $\eta_{\mathrm{Au}} = 10^{-3}$, $\eta_{\mathrm{glue}} = 10^{-3}$.

L (mm)	H (nm)	r_{glue} (μm)	f_0 (kHz)	Q_{SiN}	Q_{Au}	Q_{glue}	Q
5	50	100	1.3	$\dfrac{3 \times 10^3}{\eta_{\mathrm{SiN}}}$	$\dfrac{2.3 \times 10^5}{\eta_{\mathrm{Au}}}$	$\dfrac{2 \times 10^4}{\eta_{\mathrm{glue}}}$	17×10^6
5	100	50	1.7	$\dfrac{8 \times 10^2}{\eta_{\mathrm{SiN}}}$	$\dfrac{6 \times 10^4}{\eta_{\mathrm{Au}}}$	$\dfrac{5 \times 10^3}{\eta_{\mathrm{glue}}}$	4×10^6
5	100	100	1.9	$\dfrac{1.4 \times 10^3}{\eta_{\mathrm{SiN}}}$	$\dfrac{1.1 \times 10^5}{\eta_{\mathrm{Au}}}$	$\dfrac{8 \times 10^4}{\eta_{\mathrm{glue}}}$	7×10^6
5	100	200	2.1	$\dfrac{2 \times 10^3}{\eta_{\mathrm{SiN}}}$	$\dfrac{3 \times 10^5}{\eta_{\mathrm{Au}}}$	$\dfrac{1.1 \times 10^4}{\eta_{\mathrm{glue}}}$	11×10^6
5	200	200	2.9	$\dfrac{1.1 \times 10^3}{\eta_{\mathrm{SiN}}}$	$\dfrac{1.6 \times 10^5}{\eta_{\mathrm{Au}}}$	$\dfrac{5 \times 10^3}{\eta_{\mathrm{glue}}}$	5×10^6
1.7	50	100	1.60	$\dfrac{1.6 \times 10^3}{\eta_{\mathrm{SiN}}}$	$\dfrac{1.6 \times 10^5}{\eta_{\mathrm{Au}}}$	$\dfrac{1.3 \times 10^4}{\eta_{\mathrm{glue}}}$	11×10^6

Table I for a couple of plausible geometries. It is seen that a large glue radius and thin membrane are beneficial, and that gold losses are nearly irrelevant. The wobbling modes are affected by nearly an order of magnitude more by all the losses, and in the end they have $Q \sim 10^6$.

The high predicted Q values, acquired without exhaustive optimization of the geometry, show great promise for the experimental realization. In the discussion below, we suppose that $Q = 10^7$, which seems achievable in real life. By optimizing the contact between the membrane and the mass, one could further achieve an order of magnitude increase in Q.

C. Displacement detection

Let us recap the results for the continuous position monitoring of a single oscillator. Such a measurement is typically carried out by probing a cavity-optomechanical system at the resonant frequency of the cavity. The aim is to find out how the different known noise contributions in the gravitational force measurements will affect the sensitivity. In the deep quantum case, it turns out that the measurement quantum backaction will pose limitations for the sensitivity. It could then be beneficial to use quantum backaction evading (BAE) measurement strategies [64,65].

Below, we treat the general case where the mechanical oscillator can already be cooled, which is characterized by the effective linewidth γ and phonon occupation n_m. For example, with sideband cooling, these are given by Eqs. (2) and (3). Without any cooling, we recover the intrinsic values $n_m \Rightarrow n_m^T$, $\gamma \Rightarrow \gamma_0$. An important parameter in the discussion below is the cooperativity $\mathcal{C} = 4\mathcal{G}^2/(\kappa\gamma)$ that describes the interaction strength, and is also given in terms of the generic linewidth.

We write the linearized optomechanical Hamiltonian from Eq. (1) in terms of position x and momentum p of the oscillator, and the dimensionless quadratures x_c, y_c of the cavity:

$$H = \frac{p^2}{2M} + \frac{1}{2}M\omega_0^2 x^2 + \frac{\hbar\omega_c}{4}(x_c^2 + y_c^2) + \frac{2\hbar\mathcal{G}}{x_{\mathrm{ZP}}}xx_c. \quad (7)$$

In addition, there is a noise force $f(t) = f^L(t) + f^E(t)$ driving the oscillator consisting of the thermal plus quantum Langevin force $f^L(t)$, and of an external noise $f^E(t)$ due to environmental vibrations. The external noise $f^E(t) = M\ddot{x}^E(t)$ can be modeled as an inertial force arising from vibrations of the chip, $x^E(t)$. Writing it this way allows access to the most concrete technical noise, namely vibration noise in the refrigerator. The Langevin force has the spectral density

$$S_f^L(\omega) = 2\gamma M\hbar\omega_0\left(n_m + \frac{1}{2}\right) \equiv S_f^T + S_f^{\mathrm{ZP}}, \quad (8)$$

and the spectral density of the total force is $S_f(\omega) = S_f^L(\omega) + S_f^E(\omega)$. Above, the vacuum, thermal, and external noises are

$$S_f^{\mathrm{ZP}}(\omega) = \gamma M\hbar\omega_0, \quad (9a)$$

$$S_f^T(\omega) = 2\gamma M\hbar\omega_0 n_m, \quad (9b)$$

$$S_f^E(\omega) = M^2\omega_0^4 S_x^E(\omega), \quad (9c)$$

and $S_x^E(\omega)$ is the spectral density of cryostat vibrations.

We use the standard input-output modeling of the optomechanical cavity, with the equations of motion

$$\dot{x}_c = -\frac{\kappa}{2} + \sqrt{\kappa} x_{c,\text{in}}, \tag{10a}$$

$$\dot{y}_c = -\frac{2\mathcal{G}}{x_{\text{ZP}}}x - \frac{\kappa}{2} + \sqrt{\kappa} y_{c,\text{in}}, \tag{10b}$$

$$\dot{x} = \frac{p}{m}, \tag{10c}$$

$$\dot{p} = -m\omega_0^2 x - \frac{2\hbar\mathcal{G}}{x_{\text{ZP}}}x_c - \gamma p + f(t). \tag{10d}$$

We suppose that the cavity mode is at zero temperature, and that the cavity input noises $x_{c,\text{in}}, y_{c,\text{in}}$ have the spectrum

$$S_{x,\text{in}}(\omega) = S_{y,\text{in}}(\omega) = \tfrac{1}{2}. \tag{11}$$

We further suppose the bad-cavity limit $\kappa \gg \omega_0$, which is also relevant for the experiment, and a fully overcoupled cavity. In this scheme, the cavity y_c quadrature measures the oscillator position x, and the measurement backaction affects p directly, and also x via their coupling. All the forces enter via the mechanical susceptibility

$$\chi_m(\omega) = \frac{1}{M(\omega_0^2 - \omega^2 - i\gamma\omega)}, \tag{12}$$

that is, their effect is the strongest on resonance. The spectral density of the position fluctuations becomes

$$S_x(\omega) = |\chi_m|^2 S_f(\omega) + |\chi_{\text{qba}}|^2 S_{x,\text{in}}(\omega)$$
$$\equiv S_x^{\text{ZP}} + S_x^T + S_x^E + S_x^{\text{qba}}. \tag{13}$$

In Eq. (13), the result is sorted into contributions by the zero-point mechanical noise S_x^{ZP}, the thermal noise S_x^T, the vibration noise S_x^E, and the backaction noise S_x^{qba}:

$$S_x^{\text{ZP}} = \gamma M \hbar \omega_0 |\chi_m|^2, \tag{14a}$$

$$S_x^T = 2\gamma M \hbar \omega_0 n_m |\chi_m|^2, \tag{14b}$$

$$S_x^E = S_f^E(\omega)|\chi_m|^2, \tag{14c}$$

$$S_x^{\text{qba}} = \tfrac{1}{2}|\chi_{\text{qba}}|^2. \tag{14d}$$

The quantum backaction susceptibility grows with the measurement strength (cooperativity):

$$\chi_{\text{qba}} = 2\sqrt{\mathcal{C}\gamma}\hbar\chi_m. \tag{15}$$

We now turn to discussing how the mechanical noise spectra appear as an apparent measurement sensitivity after

detection. The output field that leaks out from the cavity replicates the oscillator position. It is given by

$$y_{c,\text{out}}(t) = \sqrt{\kappa} y_c(t) - y_{c,\text{in}}(t) = y_{c,\text{in}}(t) - \frac{2\sqrt{\mathcal{C}\gamma}}{x_{\text{ZP}}}x(t). \tag{16}$$

Additionally, there will be a contribution by the signal lost on the way, and in particular the noise added by the microwave amplifier. These contributions will be described by the added noise S_{add} in units of quanta. The amplified and detected spectrum becomes

$$S_{y,\text{out}}(\omega) = \frac{1}{2} + \frac{4\mathcal{C}\gamma}{x_{\text{ZP}}^2}S_x(\omega) + S_{\text{add}}. \tag{17}$$

We can rearrange Eq. (17) in order to secure the inferred force noise spectrum,

$$S_f^{\text{eff}}(\omega) \equiv \frac{x_{\text{ZP}}^2}{4C\gamma|\chi_m|^2}S_{y,\text{out}}(\omega)$$
$$= S_f^{\text{ZP}} + S_f^T + S_f^E + S_f^{\text{qba}} + S_f^{\text{imp}}. \tag{18}$$

Here, the backaction noise S_f^{qba} and the imprecision noise S_f^{imp} read

$$S_f^{\text{qba}} = \frac{2\mathcal{C}}{x_{\text{ZP}}^2}\gamma\hbar^2, \tag{19a}$$

$$S_f^{\text{imp}} = \frac{1/2 + S_{\text{add}}}{4\mathcal{C}\gamma|\chi_m|^2/x_{\text{ZP}}^2}. \tag{19b}$$

The standard quantum limit (SQL) indicates the minimum noise that results from the competition between improving imprecision and increasing backaction while cooperativity becomes larger. Zero temperature is assumed, as well as a noiseless single-quadrature readout of the output field. The latter implies that $S_{\text{add}} = 0$. The frequency-dependent and resonant SQLs are

$$S_f^{\text{SQL}}(\omega) = \gamma M \hbar \omega_0 + \frac{\hbar}{|\chi_m(\omega)|}, \tag{20a}$$

$$S_f^{\text{SQL}}(\omega_0) = 2\gamma M \hbar \omega_0, \tag{20b}$$

respectively. The latter states that the added noise equals at best the vacuum noise. Using a backaction evading measurement, the backaction contribution in Eq. (18) is eliminated, and the SQL is no longer a limitation. The inferred force noise in the BAE measurement becomes

$$S_f^{\text{BAE}} = S_f^{\text{ZP}} + S_f^T + S_f^E + S_f^{\text{imp}}. \tag{21}$$

D. Observing gravitational force between two oscillators

Gravitational force is often negligible in physical or chemical processes at the submillimeter scale, not to mention gravitational interaction between particles under that regime. The latter is not surprising given the fact that the electrostatic force between, e.g., a proton and electron is around forty orders of magnitude larger than the gravitational force between them. These numbers seem to indicate that it is utterly impossible to observe gravitational interactions between small particles or even everyday objects, since gravity appears to be totally masked by much stronger electromagnetic forces. This, however, is actually not the case, as hinted already by the Cavendish experiment and later work [27–30]. The reason clearly is that electromagnetic fields tend to become confined inside atoms or molecules, or canceled in conducting systems, but gravity cannot be blocked.

According to Newton, the gravitational force between two equal masses M with center-of-mass (COM) distance D is

$$F_G = \frac{GM^2}{D^2}. \tag{22}$$

Here, $G \simeq 6.67 \times 10^{-11}$ N (m/kg)^2. For example, the gravitational force is $F_G \sim 0.1$ fN between gold spheres weighing $M \sim 1$ mg and separated by $D \sim 1$ mm. Interestingly, this magnitude is well above a detection threshold given the extreme force sensitivities obtained with nanomechanical mass sensors [66]. Although the latter are not relevant for the present problem, the benchmarking gives an indication that measuring such tiny forces is in principle possible. As a static force, however, one cannot distinguish it from other forces, but a suitable modulation that uses resonant enhancement of a test mass motion could accomplish the measurements. Such a proposal was presented in Ref. [35]. In our work we translate the scheme into cryogenic microwave optomechanics, and first analyze the prospects of seeing the self-gravity with milligram masses, also considering the quantum limits of detection.

Recall the scheme in Fig. 1(a). Both membranes mass loaded by gold spheres have the same frequency ω_0. Let us call one of the masses the source mass (S). Its motion is actuated sinusoidally by an amplitude dx_S, and near resonantly (frequency ω_G). The test mass (T) will then feel the time-dependent gravitational force dF_G with

$$2dF_G(t) = -|dF_G| \sin(\omega_G t), \tag{23a}$$

$$|dF_G| = \frac{2GM^2}{D^3} dx_S, \tag{23b}$$

and respond at the motion amplitude

$$dx_T = \frac{2GM}{\gamma \omega_0 D^3} dx_S. \tag{24}$$

For example, at $Q = 10^7$ and $dx_S = 1$ μm, we have $dx_T \simeq 35$ fm, which is nearly 3 orders of magnitude larger than the zero-point amplitude. Much better imprecisions have been reached with optics [67,68], and also with microwaves [69], so the measurement sounds plausible, although it will be heavily challenged by the mechanical thermal noise, as discussed next.

The spectral density of the sinusoidal force in Eq. (23a) is $S_G(\omega) = (\pi/2)|dF_G|^2 [\delta(\omega + \omega_G) + \delta(\omega - \omega_G)]$. In the measurement this is integrated over the frequency, yielding the signal power $P_G = (\pi/2)|dF_G|^2$. This should be compared to the effective force noise power, Eq. (18), when recorded within a bandwidth B:

$$P_F = S_f^{\text{eff}}(\omega_G)B \simeq S_f^{\text{eff}}(\omega_G)\tau^{-1} \tag{25}$$

with $\tau \simeq B^{-1}$ the corresponding measurement time. Equation (25) gives the average value of the noise power. However, this is not directly the relevant figure of merit determining the possibility to see a signal peak in the detected spectrum, but instead the peak should be compared to the "noise of noise" σ_F, viz., the standard deviation of fluctuations of the average power. When averaging spectra calculated from a digitized data stream, σ_F behaves as $\tau^{-1/2}$. Now, instead, we have a coherent signal that can beneficially be recorded in a single continuous stream. In the latter case, σ_F is independent of τ, but the signal builds up coherently, $P_G \propto \tau$, leading to a much more favorable scaling. Incidentally, Eq. (25) can be interpreted to hold for σ_F by the replacement $P_F \Rightarrow \sigma_F$, if one thinks that the signal stays constant. The relevant signal-to-noise ratio is then

$$\text{SNR} = \frac{P_G}{\sigma_F} \simeq \frac{|dF_G|^2}{S_f^{\text{eff}}(\omega_G)}\tau. \tag{26}$$

For details, see the Appendix.

At this point we give a list of experimental parameters used in the rest of the paper for evaluating the experimental opportunities; see Table II. The force noise with these parameters, and with a measurement time $\tau = 1$ h, is plotted in Fig. 3 as a function of frequency around the mechanical peak. Although the mechanical noise and susceptibility have opposite effects on the sensitivity independent of frequency, the best sensitivity is reached on resonance because the imprecision noise plays the least role there. At a better imprecision noise, the frequency dependence becomes less pronounced and the measurement hence perhaps easier. Otherwise, a near-quantum-limited amplifier in this example is not important because of the overwhelming mechanical thermal noise.

TABLE II. Plausible experimental parameters. We list the parameters [refer to Fig. 1(a)] used in estimating the prospects, unless other parameters are provided in the discussion. It is likely that the mentioned g_0 values can be increased by optimizing the cavity geometry.

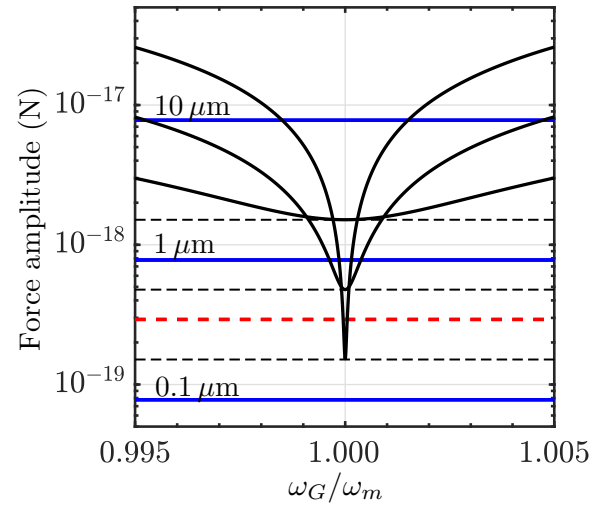| Symbol	Description	Value
L	Membrane width	5 mm
H	Membrane thickness	100 nm
R	Gold sphere radius	250 μm
M	Gold sphere mass	1.3 mg
ω_0	Mechanical resonance frequency	$2\pi \times 1.9$ kHz
x_{ZP}	Mechanical zero-point amplitude	60 am
D	Center-of-mass distance of spheres	700 μm
h_S	Vacuum gap at source oscillator	1.5 μm
h_T	Vacuum gap at test oscillator	0.5 μm
A	Electrode surface area	$(300\ \mu\text{m})^2$
$g_{0,S}$	g_0 of source oscillator	$2\pi \times 54$ mHz
$g_{0,T}$	g_0 of test oscillator	$2\pi \times 0.17$ Hz
ω_c	Microwave cavity frequency	$2\pi \times 7$ GHz
T	Equilibrium mode temperature	20 mK
n_m^T	Equilibrium phonon number	2.2×10^5
Q	Mechanical Q value, both oscillators	10^7
γ_0	Mechanical linewidth, both oscillators	$2\pi \times 0.2$ mHz
Γ	Mechanical decoherence rate	$2\pi \times 40$ Hz

FIG. 3. Sensitivity to gravitational actuation. The black curves illustrate the effective force noise, Eq. (18), at three different mechanical Q values ($Q = 10^6$, 10^7 10^8, from top to bottom at the center). The dashed horizontal black lines are the corresponding thermal plus vacuum spectra, Eq. (8), which meet the corresponding peak on resonance. The red horizontal dashed line is the contribution by external vibration noise with $\sqrt{S_x^E} = 10^{-19}/\sqrt{\text{Hz}}$. The solid horizontal blue lines are the gravitational signal S_G from the displacements dx_S as labeled. The added noise is $S_{\text{add}} = 10$ quanta. Cooperativity $\mathcal{C} = 10^2$ and the integration time $\tau = 1$ h.

We also plot in Fig. 3 the predicted gravitational signals $\sqrt{P_G}$ at different excitation amplitudes dx_S of the source mass. If the effective force noise is below the gravitational signal (SNR > 1), the latter is observable. We see that near resonance, an amplitude $dx_S = 1$ μm exposed to our default $Q = 10^7$ oscillator provides SNR > 1 within a very reasonable integration time. It could even be possible to reach down to $dx_S = 100$ nm if $Q \sim 10^8$ (which may not be realistic), or by integrating several days.

E. Gravitational forces in a system of quantum oscillators

As mentioned, measuring gravity from a source mass that is in a spatially separated superposition will be out of reach still for quite a while, although levitated nanoparticles [70,71] are showing promise to this end. The first logical steps towards experimental tests of such a genuine quantum gravity would be to study gravity in a system that exhibits some macroscopic quantum properties of massive objects. The latter could include the test mass, the source mass, or both. The states under consideration are pure states that are displaced by the gravitational field. A list of foreseeable possibilities, in an expected order of experimental difficulty, could be as follows.

(1) Ground-state cooling of the test mass oscillator.
(2) Ground-state cooling of the source mass oscillator.

(3) Squeezing of the test mass oscillator.
(4) Squeezing of the source mass oscillator.
(5) Prepare the system of both oscillators in a two-mode squeezed state.

In cases (1) and (3), the test mass oscillator's state is close to a pure quantum state. In the sense that the gravity is from an equally small source mass, the situation is more quantum plus gravitational than atomic particles in Earth's gravitational field [23–26]. In case (3), moreover, the test mass state exhibits some nonclassical properties. In case (2), gravity is produced by a source mass whose fluctuations are localized at the vacuum level. In case (4), the gravity is produced by a source whose position is in a nonclassical state. Case (5), as a genuinely entangled and nonseparable state [72], is the most nonclassical, and exhibits nonlocality and gravity at the same time. Ideally, the actuation of the source mass does not spoil the entanglement of the fluctuations.

Below, we review some protocols discussed in the literature for preparation of these states, and discuss the experimental challenges. We begin with dissipative protocols that create stabilized states, but require a high quality factor of the cavity. We then review alternative solutions that work optimally in the bad-cavity limit $\kappa \gg \omega_0$. We find that cooling via measurement appears the most promising

method to operate our oscillators in the quantum regime given most plausible experimental parameters.

1. Reservoir engineering via cavity driving

A common protocol to prepare mechanical oscillators into motional quantum states is reservoir engineering, including sideband cooling, and single-mode [73] and two-mode [74–78] squeezing. The reservoir is constructed from the optomechanical cavity, with the interaction carefully designed via a suitable pumping such that the oscillator sees a dissipative bath that pulls the oscillator into an interesting stabilized state.

A challenge in the current case is that dissipative protocols are ideally devised for the good-cavity limit $\kappa \gg \omega_0$, which is difficult to reach with 2 kHz oscillators. Empty superconducting 3D cavities [79], or those with only a small chip occupation volume [80], can attain the needed range. However, with SiN microwave optomechanics, internal cavity losses have not reached below about 20 kHz [58,81], likely due to the bulky chip assemblies that occupy a large fraction of the mode volume.

Sideband cooling and other dissipative protocols [see the bad-cavity correction term in Eq. (3)] work reasonably well if $\omega_0 \simeq \kappa$. This "not-bad-cavity" situation can be in reach experimentally. To begin with, we suppose that $\kappa = \omega_0 = 2\pi \times 2$ kHz is possible, and evaluate predictions for cooling and squeezing using our set of parameters. The stated cavity losses can be clearly dominated by internal losses, but because some signal is lost, in that case a longer averaging time or better amplifier is needed. Verification of the oscillator's status can be done using the same techniques used earlier in the corresponding experiments, and hence we do not discuss the specifics of the detection.

We remark here that in cases (1)–(4) listed below, the source and test oscillators will be in their separate 3D cavities (see Sec. III B 1), and operations on either oscillator are less likely to disturb one another in comparison to case (5) where the oscillators are coupled to the same cavity mode.

(1) Sideband *cooling the test mass oscillator to the ground state*, $n_m \lesssim 1$, is very achievable. From Eq. (3) we obtain $n_m \simeq 1.0$ using $\Gamma_{\text{opt}}/2\pi \simeq 50$ Hz and a very small input microwave power of less than 1 pW. The source mass needs to be optomechanically accessible in only a minimal amount such that it can be characterized, and its vacuum gap can be large, say $h_S \sim 10\ \mu$m, or even larger if needed.

(2) *Cooling the source mass oscillator to the ground state* requires the source oscillator to be well coupled to its cavity mode, i.e., the vacuum gap to the antennas should be as small as possible to have a decent g_0. At the same time, the vacuum gap h_S should be large enough to avoid crashing the actuated membrane into its antenna chip. As a compromise, we choose $h_S = 2\ \mu$m. An additional challenge is to induce a large enough dx_S now that

the source oscillator has a considerably increased damping. Based on the discussion in Sec. III B 2 below, the latter is deemed possible. Ground-state cooling becomes possible at a modest $P_{\text{in}} \sim 50$ pW.

Dissipative quantum *squeezing* of a mechanical oscillator is carried out using double-sideband pumping of the cavity [73,82–84]. In order to (3) *prepare the test oscillator in a squeezed state*, we use the results including bad-cavity corrections from Ref. [85]. Squeezing of about 1.5 dB is expected with our parameters, and at effective coupling of the red-detuned tone of $2\pi \times 400$ Hz, and with an optimized pump power ratio. (4) *Preparing the source oscillator in a squeezed state* is otherwise similar, but since g_0 is smaller, a higher input power of about 10 pW is needed.

(5) We consider the creation of *two-mode squeezing*, or *entanglement* of the gravitating system the most challenging technically. Dissipative protocols require at least a not-bad-cavity situation, but this will be demanding in the present case where we have to couple both oscillators to the same cavity mode, while keeping the oscillators physically separated (see Sec. III B 1). Therefore, dissipative protocols, which are well understood in standard electromechanical systems, require a cavity design that we currently do not have available. An additional challenge is that the oscillators should ideally be spaced in frequency by at least about $0.1 \times \kappa$ such that they see a different bath, which conflicts with an efficient actuation that favors equal frequencies.

Nonetheless, we evaluate the prospects using our parameters (Table II), using standard analysis [46,77]. We find that entanglement characterized by the Duan quantity is possible, for example, at $\kappa/2\pi = 2$ kHz, and with the mechanical frequencies differing by 15%. A solution for the issue with mismatched mechanical frequencies is to start the process from a heavily damped situation (recall that the dissipative protocols' performance is proportional to the decoherence rate $\Gamma = \gamma_0 n_m^T$ that is not affected by, e.g., sideband cooling), which allows actuation even when the frequencies are different.

2. Ground-state cooling by measurement-based feedback

Damping the oscillator by applying feedback built upon the measurement record, dubbed cold damping, is a popular cooling strategy in optical cavity optomechanics [17,67,68,86–89]. To obtain fast measurements, one needs here $\kappa \gg \omega_0$ that is a natural parameter regime in the current case. A challenge with entering the quantum regime with feedback is that the measurements have to track the mechanics at the decoherence rate Γ, which is the rate at which a phonon is transferred with the environment. The corresponding measurement rate is $\Gamma_{\text{meas}} = 4\eta\mathcal{G}^2/\kappa = \eta\Gamma_{\text{opt}}$, where η is the detection efficiency. With

ideal detection, $\eta = 1$. Suboptimal efficiency is due to signal losses in a lossy cavity ($\eta_{\text{int}} = \kappa_{\text{ext}}/\kappa$), and those due to detection noise (η_{add}). The total contribution is $\eta = \eta_{\text{int}}\eta_{\text{add}}$. With microwaves, η_{add} is related to the amplifier added noise S_{add}. Systems with Josephson traveling wave parametric amplifiers (JTWPAs) have reached a system $\eta_{\text{add}} \sim 50\%$ [90], which is the number we use below. To reach the quantum limit, particularly to cool to the ground state, strong measurements are required: $\Gamma_{\text{meas}} > \Gamma$.

(1) *Cooling the test mass oscillator to the ground state* is possible with the parameters given in Table II. We find [91] that $n_m < 1$ is reached, for example, with $P_{\text{in}} = 0.1$ nW, $\kappa/2\pi = 40$ kHz, which provide $\Gamma_{\text{meas}}/2\pi \simeq 100$ Hz. At $\kappa/2\pi = 200$ kHz, ground-state cooling is also possible, but requires $P_{\text{in}} = 1$ nW.

(2) *Cooling the source mass to the ground state*, $n_m < 1$, is feasible as well, although a smaller g_0 necessitates a higher $P_{\text{in}} = 1$ nW, with $\kappa/2\pi = 40$ kHz.

(3)–(5) *Squeezing* using feedback [92,93] requires interaction that currently is not available. However, squeezing can also in principle be created by combining feedback cooling and parametric modulation [94,95]. The latter can be implemented (see Sec. III B 2 below) by the same means as mechanical actuation.

3. Pulsed techniques

Preparation of conditional mechanical quantum states using a few very strong measurement pulses has been proposed [96,97] and realized in a classical situation [98,99]. In a single run, the measurement projects the state of the oscillator according to the selected protocol, and the performance is highly insensitive to the thermal population. The measurement pulse should be much shorter than the mechanical period, which requires a fast cavity response, i.e., the bad-cavity limit $\kappa \gg \omega_0$. The important parameter in these techniques is the pertaining measurement strength given as $\chi \simeq 4\sqrt{\eta}\mathcal{G}/\kappa$. While promising in principle, the requirement for strong measurements $\chi > 1$ is prohibitive for reaching the quantum regime in this technique. Note that very low-frequency mechanical oscillators, such as ours, are beneficial because the requirement of large κ is strongly relaxed, while the reachable effective coupling $\mathcal{G}$ is less sensitive to the oscillator frequency. Let us assume that $\kappa_{\text{int}} = \kappa_{\text{ext}} = 2\pi \times 20$ kHz and that the input microwave power $P_{\text{in}} = 10$ nW. The power level is otherwise not a problem but necessitates careful canceling of the pump before the JTWPA.

(1) *Ground-state cooling of the test mass oscillator*. The parameters yield $\mathcal{G} \sim 2\pi \times 20$ kHz and $\chi \sim 1$.

(2) *Ground-state cooling of the source mass oscillator*. At the same parameters, we can reach $\chi \sim 0.4$.

It seems nonetheless that obtaining $\chi > 1$ maybe challenging to reach, at least for both oscillators, due to the

power handling capability of microwave cavities. In particular, exceeding the threshold for the case of the source oscillator would require a very high pump photon number $n_P \sim 10^{10}$ that is well above $n_P \sim 10^7$ usually used in planar microwave optomechanics. At the same time we remark that 3D cavities accept much more power, and also that the pump is on only a fraction of the time such that heating is strongly suppressed. However, the combination of a very low frequency and a still decent g_0 allow for a χ an order of magnitude higher than what is realistically possible with drumhead oscillators, or with bare SiN membranes.

A stroboscopic measurement involves repeating the fast measurements synchronized with the mechanical period. It was introduced as a means to carry out quantum backaction-evading measurements [100]. The scheme was discussed in detail recently in Ref. [101]. The authors found that the requirement for the measurement strength can be relaxed in this case. The condition for hitting the quantum regime then reads, according to Ref. [101], $\chi \gtrsim \sqrt{2\pi n_m^T/Q}$, which with our parameters becomes $\chi \gtrsim 0.4$. Based on this analysis, strong enough stroboscopic measurements seem in reach. They can be used for (1)–(2) *ground-state cooling*, (3)–(4) *single-mode squeezing*, as well as for (5) *two-mode squeezing* of two degenerate oscillators, with properly timed pulse sequences.

As a summary of this section, reservoir engineering for operation in the quantum regime is possible, but requires experimental progress to reduce the cavity losses by an order of magnitude from the state of the art. With currently or reasonably likely available parameters, cooling by measurement seems the most promising method for creation of the quantum states in the very low frequency oscillators.

4. Detection of the gravitational signal in the quantum limit

Detection of the gravitational signal in a quantum oscillator system can be different from that in the thermal limit. We assume an oscillator that has been dissipatively cooled close to the ground state, $n_m = 1$. At our parameters (see Table II), the effective linewidth is then $\gamma/2\pi \approx 50$ Hz [see, e.g., Eq. (3)]. One should bear in mind that although dissipative cooling reduces the noise, the responsivity to external forces is reduced similarly. In other words, the product γn_m in Eq. (9b) at best stays unchanged in cooling, so that in the stationary case, force sensitivity is not enhanced (see, however, the discussion on nonstationary detection [102]). In practical work, however, such broadening of the very sharp peak is highly beneficial, offering relaxed tolerances for driving frequencies, and stability to drift. Also, via Eq. (14c), the sensitivity to external vibration noise is reduced, too.

We plot the force sensitivity for the cooled oscillator in Fig. 4. Because mechanical noise is nearly absent, the
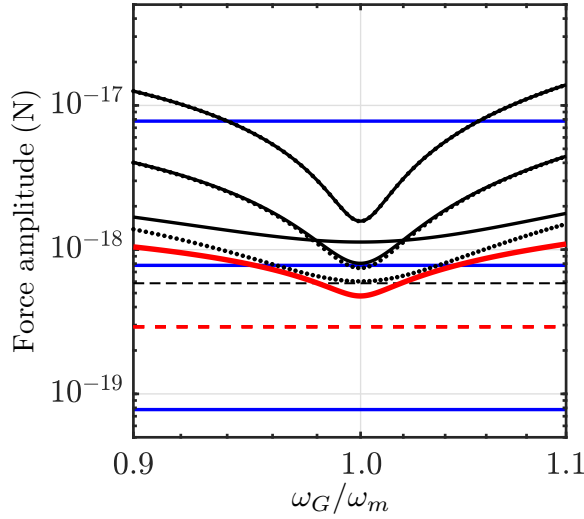
FIG. 4.   Force sensitivity of a dissipatively cooled oscillator ($n_m = 1$). The solid black curves are the effective mechanical noise, Eq. (18), at different cooperativities ($\mathcal{C} = 0.01, 0.1, 1$, from top to bottom). Additionally, the SQL [Eq. (20a)] is plotted with a thick red line, and the dotted lines depict the results from BAE monitoring [Eq. (21)] at the same cooperativities as the adjacent solid line. The horizontal lines are as in Fig. 3. The mechanical $Q = 10^7$ in all cases, and the added noise is 1 quantum. Note that the mechanical linewidth $\gamma \gg \gamma_0$ here is that resulting from the cooling, which also broadens the response in comparison to Fig. 3.

imprecision noise and also backaction noise start to play a role. Indeed, by comparing to Fig. 3, it can be seen that, with standard (non-BAE) measurements, the signal-to-noise ratio is reduced as compared to the thermal limit. A good amplifier with $S_{add} \lesssim 1$ is needed to get within a factor of 2 from the remaining thermal noise limit, but going further than that one needs BAE measurements. In Fig. 4 we also display the SQL as a red line. This is the best one can get without BAE monitoring when the oscillator is cooled to the ground state.

Feedback-based state preparation induces cooling via enhanced damping in a manner very similar to sideband cooling—the decoherence rate Γ can be assumed to stay essentially unchanged. Thus, the corresponding sensitivity is similar to that discussed immediately above, and displayed in Fig. 4.

If the oscillator quantum state is prepared based on a strong measurement, its state is being measured and known at the precision given by the zero-point motion scale, which is an order of magnitude better imprecision than the displacement given by the gravitational actuation. However, the oscillator is not cooled in the time-averaged sense, and the sensitivity is still limited by the thermal noise. An estimate of the sensitivity for measuring the gravity with an oscillator prepared by measurement is thus that displayed in Fig. 3.

III. ENGINEERING ASPECTS

A. Chip assembly

Drawings of the proposed chip assemblies are shown in Fig. 1. The test and source mass side chip assemblies are quite similar. The membrane chips are glued to their respective antenna chips. It would be tempting to proceed by rigidly attaching the two assemblies together with the gold spheres facing one another. We could not find by FEM simulations, however, a realistic way to do this without causing excessive stray mechanical coupling of the actuation into the test mass. Hence, it is better that each of the assemblies resides in their individual cavity block, which are brought close enough by nanopositioning.

B. Electromagnetic design

1. Cavity

The design of the 3D cavity is straightforward for the cases where individual cavities for the two oscillators can be used. However, in contrast to the chip assembly being in the center of the cavity [57,58], now it will be close to the wall facing the other cavity, and the wall needs to be much thinner (clearly below 100 μm) than what typical bulky cavities exhibit.

Coupling both oscillators to the same cavity mode, as needed for creation of two-mode squeezed states, is more involved. It is in principle possible to confine a cavity mode inside a (partially open) volume defined by two physically separated half-cavity blocks having an opening at the sides facing one another. A shield in the center partially covers the opening, as shown in Fig. 5. The challenge is to contain the cavity mode within the desired volume. With the complicated chip assemblies near the openings, the fields exhibit leakage that limits the cavity losses. Thus far, we are not able to find a geometry where this would become insignificant given reasonable design error margins, and typically radiation losses limit the linewidth in the range $\gtrsim 100$ kHz. Thus, reaching the good-cavity limit in this scheme is not readily available.

2. Source mass actuation

The source oscillator should include a frequency tuning capability in order to roughly match the mechanical frequencies. This is required for reaching a straightforward resonant actuation of the source mass, which is also felt resonantly at the test mass oscillator. The tuning can be accomplished in a standard manner by a constant voltage V_{dc} applied to the antenna electrode. On top of the dc voltage, there is a resonant ac voltage V_{ac}. These two cause an electrostatic driving force amplitude

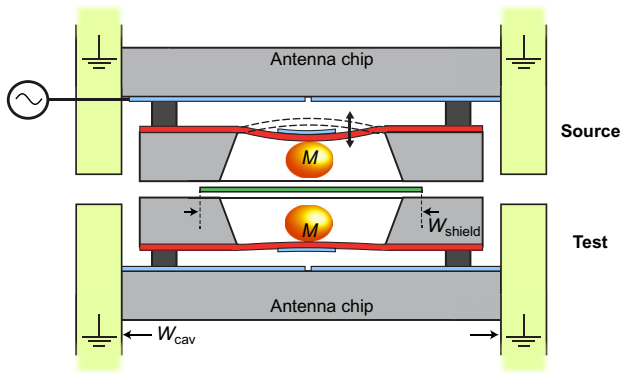$$F_S = V_{ac} V_{dc} \frac{dC_S}{dx}, \tag{27}$$

FIG. 5. Open cavity. The individual parts and the color coding correspond to Fig. 1. Two oscillators are coupled to the same cavity mode, which extends over the two separate blocks, for creation and detection of collective mechanical states. The grounded shield (green) partially isolates the two blocks. The gap between the blocks is less than a millimeter, while the chips can extend closer to one another.
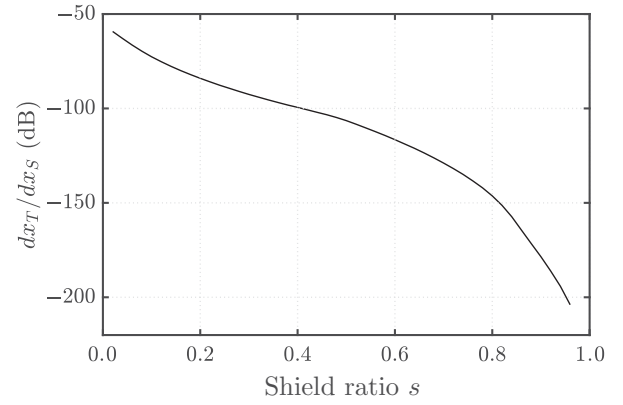

FIG. 6. Stray electrical coupling in an open cavity. The plot shows the stray coupling due to electrostatic actuation as a function of a shield coverage fraction. The data are obtained from the electric potentials at the source mass versus that of the test mass.

and the actuation amplitude becomes $dx_S = F_S/(\gamma \omega_0)$. Here, C_S is the capacitance between the antennae and the membrane electrode. If the source oscillator is not optomechanically damped (i.e., $\gamma = \gamma_0$), we find that, for example, modest values $V_{ac} = 1$ mV, $V_{dc} = 0.1$ V provide $dx_S \sim 1$ μm. However, the situation changes if the source oscillator is sideband cooled close to the ground state, and for the same amplitude, we need, e.g., $V_{ac} \sim 2$ V, $V_{dc} \sim 10$ V. The latter are high values as compared to the normal range in superconducting nanoelectronics, but we still consider them manageable. Another possibility is to use a piezo shaker for actuation, instead of electrostatic actuation.

It is critical to make sure that a false positive gravitational signal is not triggered by stray coupling of the source mass actuation into the test mass oscillator. The stray coupling of mechanical actuation has to be much smaller than the corresponding gravitational signal, Eq. (24). The ratio dx_T/dx_S is typically about -140 dB with our parameters. One channel of stray coupling is via the electrical driving. In the suggested experiments, besides the preparation of two-mode squeezed states, the two oscillators are naturally living in their own very nearby 3D cavities, which provide an extreme isolation against stray coupling of low-frequency electric fields. Below we present a design that describes by far the most demanding situation, that of using a single cavity mode for both oscillators, as needed for two-mode squeezing.

The schematics of the open cavity, Fig. 5, also shows the grounded metallic shield positioned in the middle of the cavity, between the two spheres. The shield covers a fraction $s = W_{shield}/W_{cav}$ of the opening. Here, the cavity width $W_{cav} \sim 1$ cm. Note that the antennae have to see the unshielded cavity volume in their ends in order

to couple to the collective cavity mode. From the FEM simulation, we extract the ac electric potential of the electrode beneath the gold spheres. As per Eq. (27), this gives the actuating force. We show in Fig. 6 the ratio of the resulting motion of the two spheres plus their electrode. We see that our design with about 75% of the cavity covered by the shield will be sufficient to attenuate the driving field by the required amount. We also find that at the room-temperature conductivity of aluminium the penetration of electric fields through the shielding is significantly secondary to diffraction around the shielding.

Superconductors are expected to provide even larger shielding from electric fields. A superconducting shielding thickness of 1 μm will attenuate high impedance near-field radiation by over 400 dB (more than 100 dB better than room temperature copper at the same thickness) [103]. This would suggest that, as expected, our shielding will not perform worse if the shield is superconducting. We thus conclude that stray electrical coupling can be mitigated.

C. Vibration isolation

Our situation with the design of vibration isolation has some resemblance to that for gravitational wave detectors that is well established. LIGO designs are very bulky and thus not directly applicable to our case that works at 2 kHz and needs to have a decently small footprint to fit into a dilution refrigerator. However, the resonant detector MiniGrail is an example of the latter, where above 300 dB of attenuation is claimed [104].

Isolation of our mass-loaded oscillators from vibration disturbances is critical for two reasons. There are several vibration noise sources in cryogenic systems that emit vibrations in the kilohertz frequency range, and can drive the modes into high effective temperatures (n_m^T higher than expected based on the refrigerator temperature). Second, a

mechanically coupled stay actuation from the source mass into the test mass must be mitigated.

Luckily, the frequency range of a few kilohertz is favorable for the design of the isolation. The lowest pendulum modes of typical filters that involve kilogram range masses are clearly below our range. The wavelength is large enough such that the masses or springs act as rather ideal lumped elements, and a direct brute-force FEM simulation can be used to predict the filtering of a realistic assembly. The latter is a considerable benefit since analytical modeling that can rely on heavy approximations may not properly capture the real situation.

Let us discuss the vibration noise levels in a typical pulse-tube powered dry dilution refrigerator. Vibration noise in commercial dilution refrigerators have been reported up to 1 kHz frequencies in Ref. [105]. They obtained $\sqrt{S_x^E}(1 \text{ kHz}) \lesssim 10^{-13}$ m/$\sqrt{\text{Hz}}$. From the analysis in Sec. D (see also Figs. 3 and 4), we judge a scale $\sqrt{S_x^E}(2 \text{ kHz}) < 10^{-19}$ m/$\sqrt{\text{Hz}}$. These numbers indicate that a very substantial attenuation of 120 dB between the refrigerator and the sample is required. One could expect that optimizations of the refrigerator configuration will lead to lower initial noise levels. Encouragingly, in Ref. [106], a 3 kHz oscillator was successfully thermalized down to about 30 mK when filtering was installed in a dry dilution refrigerator.

Similar to the case of electrical stray coupling (Sec. III B 2), the stray coupling of mechanical actuation has to be much smaller than the gravitational signal. The requirement is around -140 dB with our parameters. An estimate is then that there should be at least this much attenuation between the anchoring points of the two chip assemblies. We use as a criterion the attenuation between anchoring points of the 3D cavities, which is a worst-case estimate since in reality there will be attenuation between the chip and the cavity anchoring. Our isolation requirement thus becomes 120 dB between either oscillator and the refrigerator, and 140 dB between the oscillators (in the classical experiment the source oscillator does not necessarily need isolation).

Our design is shown in Fig. 7(a). The vertical bars at the top are regular support tubes of the cryostat, made of stainless steel, which is also the material we assume for the ring springs. Otherwise, the material is copper. For the FEM simulation, we assume a rigid anchoring from the top surfaces of the support tubes. The wide plate is the mixing chamber plate. Below this there are two hanging suspension assemblies, one for either oscillator. The assemblies consist of two springs and two masses. Coil springs are questionable due to the complicated mode structure they posses in our frequency range. Instead, we adapt ring springs [104,107] that also keep the assembly more rigid and easy to control in a confined space, without compromising the filtering capability. The devices are attached to the lowermost masses, and can be moved by
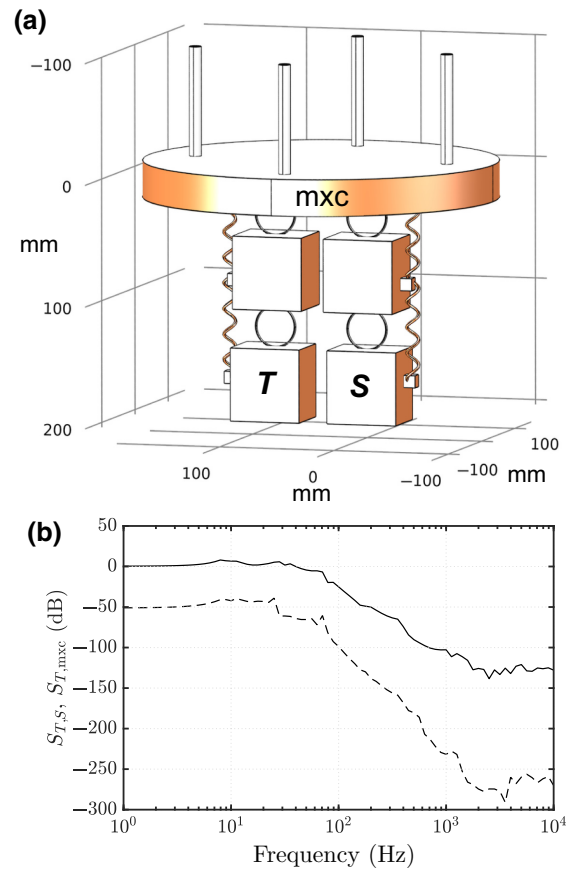

FIG. 7. Design of the suspension and vibration isolation. (a) Cavities containing the oscillators are each attached to the bottom of their own mechanical filtering systems. The filters hang from the mixing chamber plate (mxc) of the dilution cryostat. One of the filters has a cryogenic nanopositioning system (not shown). The helices model flexible thermal contacts and/or cables. The scale is in millimeters. (b) Finite-element simulation of the transfer function of displacement excitation between the mxc plate and the test mass block (solid lines), and between the test mass and source mass blocks (dashed lines).

a nanopositioning system, e.g., between the mixing chamber and the first springs. We employ a roughly optimum damping of the lowest modes, which can be realized by magnets. Asymmetry in the structure is included in order to model a realistic case. The weight of the masses of about 1.7 kg is selected such that the pendulum modes are below approximately 100 Hz. The mixing chamber plate needs to be rather massive, since otherwise its lowest flexural modes are close to the band of interest.

In Fig. 7(b) we display, first of all, the predicted attenuation between the lowermost masses of the two legs, shown with a dashed line. The attenuation between the masses around 2 kHz becomes more than 260 dB, and between the refrigerator and a single mass about 120 dB. As a result, we can conclude that a rather simple filtering

setup essentially satisfies the requirements, and leaves possibilities for development.

D. Phase noise of the microwave source

Microwave optomechanics needs ultrapure sinewave sources. High-frequency phase noise at frequencies offset from the pump by the mechanical frequency has to be suppressed below the vacuum level at the sample; otherwise, this noise will appear as an extra heating source. The suppression is normally done via room-temperature tunable cavity filters typically by the amount of tens of decibel.

In our current case, the challenge with filtering seems at first sight drastically increased as compared to, e.g., experiments with 10 MHz mechanical devices. First, the phase noise grows unavoidably towards lower frequency offsets from the pump. Second, our samples have much smaller g_0, which seems to pose a demand for high pump powers and hence more filtering since the phase noise floor is a certain amount below the pump power. Third, one needs filters with a very narrow bandwidth, down to only a few kilohertz, which is not feasible with room-temperature tunable cavities.

Let us estimate the needed filtering. The input power P_{in} and cavity photon number are related as

$$n_P = \frac{P_{in}\kappa_e}{\hbar\omega_c}\frac{1}{\Delta^2 + (\kappa/2)^2},$$ (28)

where Δ is the detuning of the pump frequency from the cavity. In the case of dissipative protocols, $|\Delta| \approx \omega_0$, and in measurement-based protocols $\Delta \approx 0$. Good commercial microwave generators have phase noise specifications at 2 kHz of about -110 dBc/Hz, which means that the noise floor is below the pump level by this amount. Now we should compare the pump power at the sample plane, at a given effective coupling, with the noise floor. We assume the bad-cavity limit, $\kappa = 10\omega_0$. Using the parameters of the test mass oscillator in Table II, we find that, in order to have a large measurement strength of about 1 kHz, the input power $P_{in} \sim 0.1$ nW. The noise floor is then about 20 dB above the vacuum level, which requires suppression by a rather modest amount of about 25 dB. The requirement is substantially relaxed if one manages to obtain a not-bad cavity situation for the dissipative protocols, and barely any filtering will be needed.

We hence find that the phase noise suppression requirement is barely affected in comparison to state-of-the-art microwave optomechanics. This is associated to the fact that in the bad-cavity limit, Eq. (28) goes as $\propto (\kappa)^{-1}$, and κ can be set according to ω_0 by the external coupling.

The still remaining issue is the need for narrow-band notch filters. They can be implemented using a tunable superconducting cryogenic cavity, which can operate in a 4 K environment.

E. Other forces

There are several forces between nearby objects that can mask the gravity. The most famous is the Casimir force, which can be very strong at small separations. Its zero-temperature expression for a sphere of radius R and a plate at a distance d, in the limit $R \gg d$, reads [108]

$$F_C = -\frac{\pi^3 \hbar c R}{360 d^3}.$$ (29)

In our experiment, the Casimir force between the source mass and the shielding varies in time. This will cause the shielding to oscillate, and in turn the Casimir force on the test mass will also vary. If the distance in Eq. (29) varies sinusoidally with amplitude dx_S around a mean value d then the time-dependent component will reduce to

$$|dF_C| = \frac{\pi^3 \hbar c R}{120 d^4} dx_S.$$ (30)

The amplitude of the oscillating force between the shielding and the test mass is strictly less than that between the source mass and the shielding, only becoming equal in the limit of the Casimir force dominating the modulus of the shielding. This allows us to calculate an absolute upper bound on the Casimir driving using Eq. (30). If the source mass is at a mean distance of $d = 100$ μm from the shielding and is sinusoidally driven with an amplitude $dx_S = 1$ μm then the amplitude of the Casimir driving will be less than 20 zN. This is 3 orders of magnitude smaller than the gravitational force for a symmetrical setup with the same dimensions.

Other forces are discussed, e.g., in Ref. [35]. One contribution is due to electrostatic patch potentials. However, they are likely not a big issue. At deep cryogenic temperatures, thermally actuated random drift of potentials is fully suppressed, while static patches do not harm the detection of a deterministic actuation. With ion traps, a strong suppression of extra heating associated to patch potential fluctuations has been observed at moderate cryogenic temperatures [109]. In the original 3D microwave optomechanics scheme with Al-coated SiN membranes, which is the same scheme we are using besides the Au spheres, ground-state cooling has been achieved [58], which shows that unaccounted noise sources are not an obstacle. Adding the gold spheres with roughly similar dimensions to the Al electrodes is not expected to enhance possible patch issues.

Another static force contribution is due to free charges. We find that on the order of 100 charges on the spheres at $d = 100$ μm separation gives a force equal to the gravity. Characterizing the amount of charges and getting rid of them in a cryogenic experiment will be difficult.

In spite of the other forces, some of which are very difficult to independently calibrate out, we foresee that they do not pose a major challenge. First, we assume that

there is a grounded conductive shield between the spheres. Similar to the case of low-frequency electric fields (see Sec. III B 2), we argue that even a partial shield is very effective at canceling these forces that occur between adjacent surfaces. Second, gravity has a unique signature that depends on the COM distance, whereas the other forces depend on the surface separation. Tuning the distance between the spheres can thus facilitate spotting the gravity.

We remark that at deep cryogenic temperatures, damping by collisions with gas molecules is not an issue. We are not aware of pressure estimates inside dilution refrigerator, but one can expect that essentially all the particles will stick upon collision owing to a vanishing vapor pressure. If the experimental volume is shielded from outside, the pressure is zero for all practical purposes.

IV. EXPERIMENT WITH A MASS-LOADED MEMBRANE

We carry out a test of a fundamental part of the proposal, namely a single membrane oscillator loaded by a 0.5 mm diameter gold sphere. The goals are to verify the predicted mode structure and to show the possibility for high mechanical Q values as predicted by simulations.

The membrane window chip we discuss below is purchased from Norcada. It is a $(1 \times 10 \times 10 \text{ mm}^3)$-sized Si chip coated by 50 nm of SiN with roughly 900 MPa tensile prestress. The SiN window is a 1.7 mm wide rectangle made using Potassium hydroxide (KOH) etch. Aluminum metallization is applied in the center of the membrane as a 200 μm circle. The antenna chips, of standard floatzone silicon, are Al metallized as well. The membrane chip is flipped on top of the antenna chip. The natural gap between the chips without any spacers in between becomes typically less than a micron, set by dust or irregularities, although in this assembly we believe the gap is of the order of a few microns. After flipping, the membrane chip is glued with epoxy from one corner, and after the epoxy has cured, firmly glued around all edges. The latter is because

we expect there can be modes involving the entire chip in the kilohertz range, if the chip is not fully anchored. The 4N gold spheres are purchased from Goodfellow. The fabrication steps are shown in Fig. 8 for a device similar to that measured. A sphere is positioned on the membrane as shown in Figs. 8(a)–8(c). The chip assembly is fixed using PMMA resist into a standard 3D copper cavity [Fig. 8(d)].

The measurements are carried out in a dry pulse-tube dilution refrigerator at around 10 mK temperature. The sample stage has a copper braid suspension, but there is no other vibration damping in the setup. We find that normal operation of the refrigerator when the pulse tube is running causes the mechanical modes to be strongly excited. Thus, the data are recorded when the pulse tube is switched off momentarily.

In Fig. 9(a) we display the measured mechanical noise spectrum over a large frequency range. The strongest peak at $\omega_0/2\pi \simeq 1.69$ kHz is identified as the desired flexural mode. The peaks below 100 Hz are likely motion of the entire chip assembly. The two smaller peaks at 580 and 690 Hz are interpreted as the two wobbling modes, which naturally have much lower optomechanical coupling. The mode profiles are also displayed in Fig. 9(a). The measured ω_0 agrees well with the result from Eq. (6) and the FEM simulation with the known parameters and the glue radius $r_{\text{glue}} = 100 \ \mu$m. The wobbling modes in a fully symmetric case are degenerate, but this is lifted by asymmetries in, e.g., the positioning of the glue and the sphere. However, by distorting the symmetry in simulations by a reasonable amount, we are not able to reproduce such a high nondegeneracy. The reason could be distortion of the chip due to thermal contraction during cool down, which is currently beyond the scope of the simulations.

The mechanical peak of the main mode is displayed in Fig. 9(b), where we plot the total spectrum $S_{\text{out}}(\omega) = S_{x,\text{out}}(\omega) + S_{y,\text{out}}(\omega)$. The Q value extracted from the fit is $Q \simeq 6.4 \times 10^5$. The Q value can be even higher, since the frequency resolution is limited by the time of approximately 5 min that we are able to run the fridge

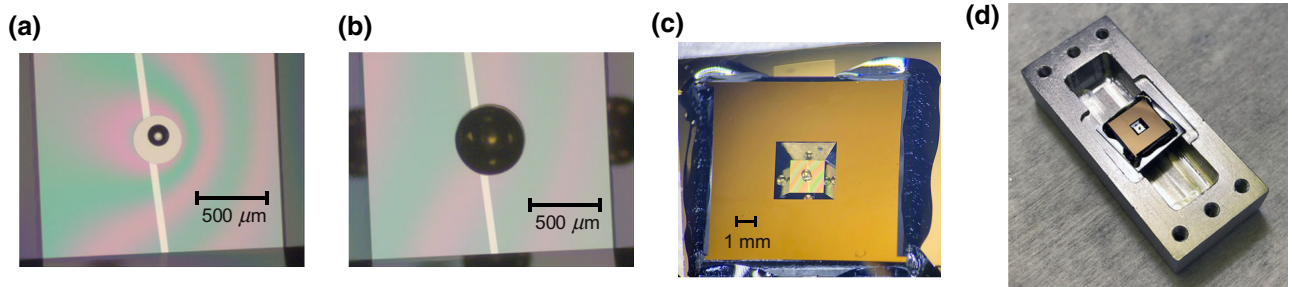

(a)   **(b)**   **(c)**   **(d)**

FIG. 8.   Preparing the sample. (a) The membrane chip with a 1.7 mm wide, 50 nm thick SiN window has been flipped on top of an antenna chip, and firmly glued into it. An epoxy glue drop about 150 μm in diameter is micropositioned in the center of the membrane on top of an Al electrode. (b) A 0.5 mm diameter gold sphere is micropositioned on top of the glue. (c) Photograph of the entire chip. Reflections of the gold sphere appear at the oblique mirrorlike sidewalls. (d) The assembled device attached to the lower half of the rectangular 3D microwave cavity.
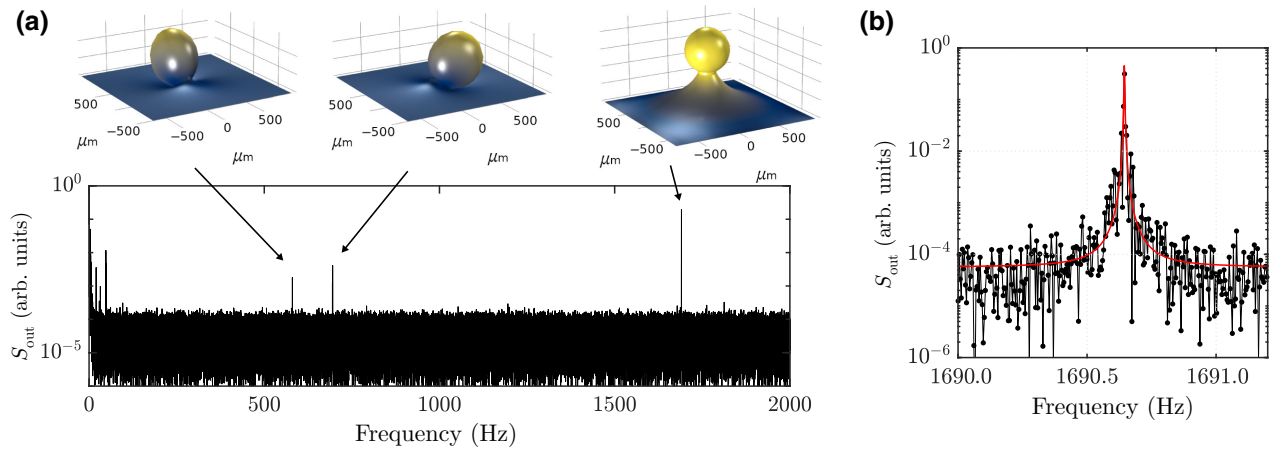
FIG. 9.   Mechanical noise spectrum at 10 mK. (a) Large frequency range with respect to the pump frequency. Three peaks interpreted as drum modes are visible. The corresponding mode profiles predicted by finite-element simulation are displayed. (b) An enlarged view of the lowest drum mode with $f_0 \simeq 1.69$ kHz and $Q \simeq 6.4 \times 10^5$. The red line is a Lorentzian fit.

without the pulse tube running. Supposing the Q is limited by losses in the adhesive, its loss factor in the idealized geometry becomes $\eta_{\text{glue}} \sim 2 \times 10^{-2}$ (see Table I). Using, e.g., PMMA [63] ($\eta \sim 10^{-3}$) as the glue, one could further improve the Q value. We also expect that the details of the glue attachment point can be optimized. It is encouraging that a simple gluing of a mass to an oscillator still allows for a Q value in the one million range, as also observed in Ref. [110].

The cavity frequency with the chip inside is 5.27 GHz, and internal linewidth 9 MHz. The latter is clearly higher than the approximate 0.3 MHz we usually observe with our standard bare 0.5 mm wide membrane chips in similar (nonsuperconducting) cavities. We do not attribute the high cavity losses to the gold spheres or the assembly in general, nonetheless. With a similar bare 1.7 mm window chip, the cavity losses are also significantly enhanced. Moreover, a standard 0.5 mm window chip loaded by the gold sphere, measured in an aluminum cavity, resulted in 0.3 MHz internal linewidth. Based on the measured cavity properties, one can see, however, that reaching the not-bad-cavity case with a few kilohertz oscillators is not straightforward.

V. CONCLUSIONS

In conclusion, we have presented a detailed experimental proposal for (1) observing gravity between milligram range masses using microwave optomechanics at deep cryogenic temperatures; (2) pushing the experiment down to the quantum limit where the positions of source mass or test mass, or both, exhibit significant quantum fluctuations. Although the massive quantum state will be created microwave optomechanically and the gravity is classical, the measurement will allow experimental studies on the overlap of quantum mechanics and gravity. One can

even foresee that, when these two disparate entities are forced closer to one another more than ever before, one can experimentally achieve a limit where fundamentally new physics may be revealed, possibly revising our understanding of quantum mechanics and gravity. Additionally, observing highly massive mechanical oscillators in the quantum regime is, in itself, an important step in this direction.

APPENDIX: SIGNAL-TO-NOISE RATIO IN THE DETECTION OF A COHERENT SIGNAL

We discuss here an important issue that is often overlooked. The question is simple: How long does one have to average a coherent signal in order to see it? The derivation below is not fully rigorous, but we hope it will clarify the issue. In order to properly analyze the situation, one has to know how the measurements are performed and processed inside an instrument (such as a spectrum analyzer). Since this information is not easy to find or digest,

we select a conceptually simple but most important measurement system: the data digitizer. It can be assumed to make instantaneous snapshots of the data stream.

We discuss the quantity $x(t)$, such as the amplified voltage from the sample. It is characterized by the correlation function $R(t)$ and the spectral density $S(\omega)$:

$$R(t) = \langle x(t_0)x(t_0 - t)\rangle_{t_0} = \frac{1}{T_0}\int_{-T_0/2}^{T_0/2} dt_0 x(t_0)x(t_0 - t),$$

$$S(\omega) = \mathcal{F}[R(t)] = \int d\omega R(t) \exp(-i\omega t). \tag{A1}$$

We suppose that the measurement of $x(t)$ is a continuous sampling that lasts over the time τ. Let us sample the quantity $x(t)$ at time intervals T. Then there are a total of $N = \tau/T$ data readings. The sampling provides the readings $x_n = x(nT)$, where n goes from 0 to $N-1$.

In order to satisfy the Nyquist sampling criterion, before sampling, the data has to be restricted to the spectral bandwidth

$$|\omega_B/2\pi| = |f_B| < (2T)^{-1} \tag{A2}$$

by analog low-pass filtering. The frequency response of an ideal low-pass filter equals the box function: $U(\omega) = 1$ when $-\omega_B < \omega < \omega_B$ and $U(\omega) = 0$ elsewhere. In the time domain, the filtering function is

$$\begin{aligned} u(t) &= \mathcal{F}^{-1}[U(\omega)] \\ &= \frac{1}{2\pi}\int d\omega U(\omega)\exp(i\omega t) \\ &= \frac{\omega_B}{2\pi}\text{sinc}(\omega_B t). \end{aligned} \tag{A3}$$

After filtering, the spectral density and the correlation function are

$$\begin{aligned} S_B(\omega) &= U(\omega)S(\omega), \\ R_B(t) &= \mathcal{F}^{-1}[S_B(\omega)]. \end{aligned} \tag{A4}$$

Below we use the following discrete correlator of the sampled data:

$$\begin{aligned} R_{nm} &\equiv \langle x(nT)x(mT)\rangle \\ &= \int dt' \delta(t' - nT)\int dt'' \delta(t'' - mT)\langle x(t')x(t'')\rangle \\ &= R_B[T(n - m)]. \end{aligned} \tag{A5}$$

For the last form in Eq. (A5), we used time translation invariance.

Aiming at obtaining the spectral density, the processing starts by evaluating the discrete Fourier transform

$$X_k = \sum_{n=0}^{N-1} x_n \exp\left(-\frac{2i\pi nk}{N}\right). \tag{A6}$$

Here, the index k refers to the frequency values. An estimate of the power spectral density $S(\omega)$ is then given by

$$S_k = \frac{1}{N}|X_k|^2 = \frac{1}{N}\sum_{n,m} x_n x_m \exp\left(\frac{2i\pi(m-n)k}{N}\right). \tag{A7}$$

Equation (A7) is known as the periodogram. The interesting figures now are the average and variance of the periodogram. The average is

$$\langle S_k \rangle = \frac{1}{N}\sum_{n,m} R_{nm} \exp\left(\frac{2i\pi(m-n)k}{N}\right). \tag{A8}$$

For evaluating the variance

$$\text{Var}[S_k] = \langle S_k^2 \rangle - \langle S_k \rangle^2, \tag{A9}$$

we need the second moment of the periodogram

$$\langle S_k^2 \rangle = \frac{1}{N^2}\sum_{n,m,p,q} \langle x_n x_m x_p x_q \rangle \exp\left(\frac{2i\pi(m-n+p-q)k}{N}\right). \tag{A10}$$

1. White noise

We now treat the case that the incoming signal is uncorrelated white noise: $R(t) = S_0\delta(t)$ and $S(\omega) = S_0$. The filtered correlation function in Eq. (A4) becomes $R_B(t) = S_0 u(t)$, with the discrete version [Eq. (A5)]

$$R_{nm} = S_0\frac{\omega_B}{2\pi}\text{sinc}[\omega_B T(n-m)] = S_0\frac{\omega_B}{2\pi}\text{sinc}[\pi(n-m)]. \tag{A11}$$

For the latter form, we used Eq. (A2). Equation (A11) is used in Eq. (A8) to evaluate the average spectrum. The sinc(y) function can be approximated to be zero at argument values $y \gtrsim 1$. Therefore, only $n = m$ gives a contribution to R_{nm}. The complex exponential in Eq. (A8) in principle makes the terms oscillate as a function of n and m. However, the condition that $n = m$ also guarantees that the exponential factor equals 1. The average value of the sampled white noise then becomes

$$\langle S_k \rangle = S_0 f_B, \tag{A12}$$

which is the anticipated result of the noise power within the bandwidth defined by the analog low-pass filter. Note

that the result does not depend on the sampling rate or the averaging time.

The fourth moment $\langle x_n x_m x_p x_q \rangle$ of the signal in Eq. (A10) can be written, using Wick's theorem, in terms of second moments, i.e.,

$$\langle x_n x_m x_p x_q \rangle = R_{nm}R_{pq} + R_{np}R_{mq} + R_{nq}R_{mp}, \quad \text{(A13)}$$

where the R_{ij} are those given in Eq. (A11). Again, in order to obtain nonzero contributions, we require that $i = j$ in all R_{ij} in Eq. (A13). The two first terms on the rhs are treated similarly as in the discussion following Eq. (A11). For the last term $R_{nq}R_{mp}$, the requirement reads, as usual, $n = q, m = p$; however, the exponent in Eq. (A10) cannot equal to zero simultaneous to this requirement. Therefore, this term gives oscillatory values whose contribution will vanish. Equation (A10) becomes

$$\langle S_k^2 \rangle = 2S_0^2 f_B^2, \quad \text{(A14)}$$

and the standard deviation is

$$\text{s.d.}[S_k] = S_0 f_B. \quad \text{(A15)}$$

Equation (A15) is the main quantity of interest. It describes the "noise of noise," fluctuations of the spectrum around the mean value around Eq. (A8). If a signal peak in the spectrum is larger than s.d.$[S_k]$, the signal becomes visible (in practice, the signal peak should be a small numerical factor larger than s.d.$[S_k]$).

Note that s.d.$[S_k]$ does *not* depend on the integration time. This seems at first sight to be in stark contrast to the intuition that uncertainty does decrease with longer integration time. In order to resolve this controversy, we have to make more detailed considerations of the measurement.

2. Coherent signal

The main model of detection of an external force is via coherent actuation of the oscillator. This is also the case in the current work. We now calculate the average spectrum, Eq. (A8), for a sinusoidal signal

$$F(t) = dF \sin(\omega_G t). \quad \text{(A16)}$$

Note that in the classical situation its variance is zero because the signal is deterministic. The continuous and discrete correlation functions are

$$R(t) = \frac{dF^2}{2} \cos(\omega_G t),$$
$$R_{nm} = \frac{dF^2}{2} \cos\left[\omega_G T(n - m)\right]. \quad \text{(A17)}$$

Since the spectrum is empty anywhere else other than at ω_G, the only requirement for the sampling rate is $f_G <$

$1/(2T)$. Moreover, the signal should pass the low-pass filter, that is, $f_G < f_B$. Given that the Nyquist criterion is satisfied, the overall criterion is $f_G < 1/(2T)$.

From Eq. (A8) we see that nonoscillatory terms will be obtained only if $k = \omega_G \tau/2\pi \equiv k_G$, i.e., at the frequency of the sinewave. At this frequency we have

$$\langle S_{k_G} \rangle = \frac{dF^2}{4N} \sum_{n,m}\{1 + \cos[2\omega_G T(n - m)]$$
$$+ i\sin[2\omega_G T(n - m)]\}$$
$$\Rightarrow \frac{dF^2}{4}N = \frac{dF^2}{4}\frac{\tau}{T}. \quad \text{(A18)}$$

Based on Eq. (A18), the power of the coherent spectral peak grows, first of all, with the integration time τ. This can be interpreted so that a long measurement implies higher frequency resolution, which allows for a more accurate construction of the delta function peak. Since the noise of noise s.d.$[S_k]$ stays constant, the signal-to-noise ratio will improve over a longer measurement, as it should.

We also see that the peak grows without limit when the sampling rate T^{-1} is increased. This again seems to contradict intuition and give an unlimited SNR by just sampling faster, since s.d.$[S_k]$ does not depend on T. However, by sampling too fast the Nyquist criterion fails to hold, and as a result, the noise grows due to aliasing, and the SNR is not improved. The optimum is reached at the threshold $f_B = 1/(2T)$, and Eq. (A18) becomes

$$\langle S_{k_G} \rangle = P_G \tau f_B, \quad \text{(A19)}$$

where $P_G = dF^2/2$ is the signal power.

After a surprisingly tedious calculation, we obtain the final result

$$\text{SNR} = \frac{\langle S_{k_G} \rangle}{\text{s.d.}[S_k]} = \frac{P_G}{S_0}\tau, \quad \text{(A20)}$$

which is essentially Eq. (26). Equation (26) is often wrongly justified by comparing the mean noise level, Eq. (A12), to the signal.

The integration time needed to make the signal visible, SNR > 1, based on Eq. (26) scales rather favorably with the noise level. In order to reach this, the detection must occur as a *single time-domain run* (or built based on trigger events). In this case, the signal adds up coherently. If one averages individual periodograms instead of averaging one long periodogram, the scaling will be $\tau \propto (P_G/S_0)^2$.

We still briefly comment on the detection of a signal peak of a finite width. This occurs when the signal is of a natural origin instead of a coherent driving signal. In cavity optomechanics, this measurement is by far more important than that using a coherent drive. Now, there is

no benefit of averaging in the time domain instead of averaging periodograms. The average noise level, Eq. (A8), reflects the original spectral lineshape, and the noise of noise, Eq. (A14), does not depend on the integration time. Where does it then appear that a longer measurement should improve the signal-to-noise ratio? A longer measurement implies more information because it increases the frequency resolution $\propto \tau^{-1}$, that is, there are more independent data points available. Adjacent frequency bins can then be processed by a moving average filter with a bandwidth less than the peak width. Such averaging of data points will then reduce the noise of noise.

---

[1] Erwin Schrödinger, Die gegenwärtige Situation in der Quantenmechanik, Naturwissenschaften **23**, 807 (1935).

[2] Markus Arndt, Olaf Nairz, Julian Vos-Andreae, Claudia Keller, Gerbrand van der Zouw, and Anton Zeilinger, Wave–particle duality of C60 molecules, Nature **401**, 680 (1999).

[3] Brian Julsgaard, Alexander Kozhekin, and Eugene S. Polzik, Experimental long-lived entanglement of two macroscopic objects, Nature **413**, 400 (2001).

[4] Y. Nakamura, Y. A. Pashkin, and J. S. Tsai, Coherent control of macroscopic quantum states in a single-Cooper-pair box, Nature **398**, 786 (1999).

[5] A. D. O'Connell, M. Hofheinz, M. Ansmann, Radoslaw C. Bialczak, M. Lenander, Erik Lucero, M. Neeley, D. Sank, H. Wang, M. Weides, J. Wenner, John M. Martinis, and A. N. Cleland, Quantum ground state and single-phonon control of a mechanical resonator, Nature **464**, 697 (2010).

[6] B. P. Abbott, *et al.* (LIGO Scientific Collaboration and Virgo Collaboration), Observation of Gravitational Waves from a Binary Black Hole Merger, Phys. Rev. Lett. **116**, 061102 (2016).

[7] Igor Pikovski, Michael R. Vanner, Markus Aspelmeyer, M. S. Kim, and Caslav Brukner, Probing Planck-scale physics with quantum optics, Nat. Phys. **8**, 393 (2012).

[8] Francesco Marin, Francesco Marino, Michele Bonaldi, Massimo Cerdonio, Livia Conti, Paolo Falferi, Renato Mezzena, Antonello Ortolan, Giovanni A. Prodi, Luca Taffarello, Gabriele Vedovato, Andrea Vinante, and Jean-Pierre Zendri, Gravitational bar detectors set limits to Planck-scale physics on macroscopic variables, Nat. Phys. **9**, 71 (2013).

[9] Alessio Belenchia, Dionigi M. T. Benincasa, Stefano Liberati, Francesco Marin, Francesco Marino, and Antonello Ortolan, Testing Quantum Gravity Induced Nonlocality via Optomechanical Quantum Oscillators, Phys. Rev. Lett. **116**, 161303 (2016).

[10] Marios Christodoulou and Carlo Rovelli, On the possibility of laboratory evidence for quantum superposition of geometries, Phys. Lett. B **792**, 64 (2019).

[11] Abdulrahim Al Balushi, Wan Cong, and Robert B. Mann, Optomechanical quantum Cavendish experiment, Phys. Rev. A **98**, 043811 (2018).

[12] Haixing Miao, Denis Martynov, Huan Yang, and Animesh Datta, Quantum correlations of light mediated by gravity, Phys. Rev. A **101**, 063804 (2020).

[13] Markus Aspelmeyer, Tobias J. Kippenberg, and Florian Marquardt, Cavity optomechanics, Rev. Mod. Phys. **86**, 1391 (2014).

[14] Roger Penrose, On gravity's role in quantum state reduction, Gen. Relativ. Gravit. **28**, 581 (1996).

[15] Brahim Lamine, Rémy Hervé, Astrid Lambrecht, and Serge Reynaud, Ultimate Decoherence Border for Matter-Wave Interferometry, Phys. Rev. Lett. **96**, 050405 (2006).

[16] O. Arcizet, P. F. Cohadon, T. Briant, M. Pinard, and A. Heidmann, Radiation-pressure cooling and optomechanical instability of a micromirror, Nature **444**, 71 (2006).

[17] B. Abbott *et al.*, Observation of a kilogram-scale oscillator near its quantum ground state, New J. Phys. **11**, 073032 (2009).

[18] J. T. Santos, J. Li, J. Ilves, C. F. Ockeloen-Korppi, and M. Sillanpää, Optomechanical measurement of a millimeter-sized mechanical oscillator approaching the quantum ground state, New J. Phys. **19**, 103014 (2017).

[19] Nobuyuki Matsumoto, Seth B. Cataño Lopez, Masakazu Sugawara, Seiya Suzuki, Naofumi Abe, Kentaro Komori, Yuta Michimura, Yoichi Aso, and Keiichi Edamatsu, Demonstration of Displacement Sensing of a mg-Scale Pendulum for mm- and mg-Scale Gravity Measurements, Phys. Rev. Lett. **122**, 071101 (2019).

[20] Seth B. Cataño Lopez, Jordy G. Santiago-Condori, Keiichi Edamatsu, and Nobuyuki Matsumoto, High-*Q* Milligram-Scale Monolithic Pendulum for Quantum-Limited Gravity Measurements, Phys. Rev. Lett. **124**, 221102 (2020).

[21] Haocun Yu *et al.*, Quantum correlations between light and the kilogram-mass mirrors of LIGO, Nature **583**, 43 (2020).

[22] C. A. Regal, J. D. Teufel, and K. W. Lehnert, Measuring nanomechanical motion with a microwave cavity interferometer, Nat. Phys. **4**, 555 (2008).

[23] R. Colella, A. W. Overhauser, and S. A. Werner, Observation of Gravitationally Induced Quantum Interference, Phys. Rev. Lett. **34**, 1472 (1975).

[24] Valery V. Nesvizhevsky, Hans G. Börner, Alexander K. Petukhov, Hartmut Abele, Stefan Baeßler, Frank J. Rueß, Thilo Stöferle, Alexander Westphal, Alexei M. Gagarski, Guennady A. Petrov, and Alexander V. Strelkov, Quantum states of neutrons in the Earth's gravitational field, Nature **415**, 297 (2002).

[25] Achim Peters, Keng Yeow Chung, and Steven Chu, Measurement of gravitational acceleration by dropping atoms, Nature **400**, 849 (1999).

[26] G. Rosi, F. Sorrentino, L. Cacciapuoti, M. Prevedelli, and G. M. Tino, Precision measurement of the Newtonian gravitational constant using cold atoms, Nature **510**, 518 (2014).

[27] Rogers C. Ritter, Charles E. Goldblum, Wei-Tou Ni, George T. Gillies, and Clive C. Speake, Experimental test of equivalence principle with polarized masses, Phys. Rev. D **42**, 977 (1990).

[28] Wen-Hai Tan, Shan-Qing Yang, Cheng-Gang Shao, Jia Li, An-Bin Du, Bi-Fu Zhan, Qing-Lan Wang, Peng-Shun Luo, Liang-Cheng Tu, and Jun Luo, New Test of the Gravitational Inverse-Square law at the Submillimeter

Range with Dual Modulation and Compensation, Phys. Rev. Lett. **116**, 131101 (2016).

[29] Wen-Hai Tan, An-Bin Du, Wen-Can Dong, Shan-Qing Yang, Cheng-Gang Shao, Sheng-Guo Guan, Qing-Lan Wang, Bi-Fu Zhan, Peng-Shun Luo, Liang-Cheng Tu, and Jun Luo, Improvement for Testing the Gravitational Inverse-Square law at the Submillimeter Range, Phys. Rev. Lett. **124**, 051301 (2020).

[30] J. G. Lee, E. G. Adelberger, T. S. Cook, S. M. Fleischer, and B. R. Heckel, New Test of the Gravitational $1/r^2$ law at Separations Down to 52 μm, Phys. Rev. Lett. **124**, 101101 (2020).

[31] J. Chiaverini, S. J. Smullin, A. A. Geraci, D. M. Weld, and A. Kapitulnik, New Experimental Constraints on Non-Newtonian Forces below 100 μm, Phys. Rev. Lett. **90**, 151101 (2003).

[32] R. S. Decca, D. López, H. B. Chan, E. Fischbach, D. E. Krause, and C. R. Jamell, Constraining New Forces in the Casimir Regime Using the Isoelectronic Technique, Phys. Rev. Lett. **94**, 240401 (2005).

[33] Cheng-Gang Shao, Yu-Jie Tan, Wen-Hai Tan, Shan-Qing Yang, Jun Luo, and Michael Edmund Tobar, Search for Lorentz invariance violation through tests of the gravitational inverse square law at short ranges, Phys. Rev. D **91**, 102007 (2015).

[34] J. C. Long and V. Alan Kostelecký, Search for Lorentz violation in short-range gravity, Phys. Rev. D **91**, 092003 (2015).

[35] Jonas Schmöle, Mathias Dragosits, Hans Hepach, and Markus Aspelmeyer, A micromechanical proof-of-principle experiment for measuring the gravitational force of milligram masses, Class. Quantum Grav. **33**, 125031 (2016).

[36] Tobias Westphal, Hans Hepach, Jeremias Pfaff, and Markus Aspelmeyer, Measurement of Gravitational Coupling between Millimeter-Sized Masses, arXiv:2009.09546 (2020).

[37] J. D. Teufel, T. Donner, Dale Li, J. W. Harlow, M. S. Allman, K. Cicak, A. J. Sirois, J. D. Whittaker, K. W. Lehnert, and R. W. Simmonds, Sideband cooling of micromechanical motion to the quantum ground state, Nature **475**, 359 (2011).

[38] Jasper Chan, T. P. Mayer Alegre, Amir H. Safavi-Naeini, Jeff T. Hill, Alex Krause, Simon Gröblacher, Markus Aspelmeyer, and Oskar Painter, Laser cooling of a nanomechanical oscillator into its quantum ground state, Nature **478**, 89 (2011).

[39] T. A. Palomaki, J. D. Teufel, R. W. Simmonds, and K. W. Lehnert, Entangling mechanical motion with microwave fields, Science **342**, 710 (2013).

[40] T. P. Purdy, R. W. Peterson, and C. A. Regal, Observation of radiation pressure shot noise on a macroscopic object, Science **339**, 801 (2013).

[41] Amir H. Safavi-Naeini, Simon Gröblacher, Jeff T. Hill, Jasper Chan, Markus Aspelmeyer, and Oskar Painter, Squeezed light from a silicon micromechanical resonator, Nature **500**, 185 (2013).

[42] V. Sudhir, D. J. Wilson, R. Schilling, H. Schütz, S. A. Fedorov, A. H. Ghadimi, A. Nunnenkamp, and T. J. Kippenberg, Appearance and Disappearance of Quantum Correlations in Measurement-Based Feedback Control of a Mechanical Oscillator, Phys. Rev. X **7**, 011001 (2017).

[43] C. F. Ockeloen-Korppi, E. Damskägg, J.-M. Pirkkalainen, T. T. Heikkilä, F. Massel, and M. A. Sillanpää, Noiseless Quantum Measurement and Squeezing of Microwave Fields Utilizing Mechanical Vibrations, Phys. Rev. Lett. **118**, 103601 (2017).

[44] David Mason, Junxin Chen, Massimiliano Rossi, Yeghishe Tsaturyan, and Albert Schliesser, Continuous force and displacement measurement below the standard quantum limit, Nat. Phys. **15**, 745 (2019).

[45] Sungkun Hong, Ralf Riedinger, Igor Marinković, Andreas Wallucks, Sebastian G. Hofer, Richard A. Norte, Markus Aspelmeyer, and Simon Gröblacher, Hanbury Brown and Twiss interferometry of single phonons from an optomechanical resonator, Science **358**, 203 (2017).

[46] C. F. Ockeloen-Korppi, E. Damskägg, J. M. Pirkkalainen, M. Asjad, A. A. Clerk, F. Massel, M. J. Woolley, and M. A. Sillanpää, Stabilized entanglement of massive mechanical oscillators, Nature **556**, 478 (2018).

[47] Ralf Riedinger, Andreas Wallucks, Igor Marinković, Clemens Löschnauer, Markus Aspelmeyer, Sungkun Hong, and Simon Gröblacher, Remote quantum entanglement between two micromechanical oscillators, Nature **556**, 473 (2018).

[48] Igor Marinković, Andreas Wallucks, Ralf Riedinger, Sungkun Hong, Markus Aspelmeyer, and Simon Gröblacher, Optomechanical Bell Test, Phys. Rev. Lett. **121**, 220404 (2018).

[49] T. P. Purdy, K. E. Grutter, K. Srinivasan, and J. M. Taylor, Quantum correlations from a room-temperature optomechanical cavity, Science **356**, 1265 (2017).

[50] V. Sudhir, R. Schilling, S. A. Fedorov, H. Schütz, D. J. Wilson, and T. J. Kippenberg, Quantum Correlations of Light from a Room-Temperature Mechanical Oscillator, Phys. Rev. X **7**, 031055 (2017).

[51] J. M. Fink, M. Kalaee, A. Pitanti, R. Norte, L. Heinzle, M. Davanço, K. Srinivasan, and O. Painter, Quantum electromechanics on silicon nitride nanomembranes, Nat. Commun. **7**, 12396 (2016).

[52] S. Barzanjeh, M. Wulf, M. Peruzzo, M. Kalaee, P. B. Dieterle, O. Painter, and J. M. Fink, Mechanical on-chip microwave circulator, Nat. Commun. **8**, 953 (2017).

[53] X. Zhou, D. Cattiaux, R. R. Gazizulin, A. Luck, O. Maillet, T. Crozes, J.-F. Motte, O. Bourgeois, A. Fefferman, and E. Collin, On-Chip Thermometry for Microwave Optomechanics Implemented in a Nuclear Demagnetization Cryostat, Phys. Rev. Appl. **12**, 044066 (2019).

[54] J. D. Teufel, Dale Li, M. S. Allman, K. Cicak, A. J. Sirois, J. D. Whittaker, and R. W. Simmonds, Circuit cavity electromechanics in the strong-coupling regime, Nature **471**, 204 (2011).

[55] J. Suh, A. J. Weinstein, C. U. Lei, E. E. Wollman, S. K. Steinke, P. Meystre, A. A. Clerk, and K. C. Schwab, Mechanically detecting and avoiding the quantum fluctuations of a microwave field, Science **344**, 1262 (2014).

[56] N. R. Bernier, L. D. Tóth, A. Koottandavida, M. A. Ioannou, D. Malz, A. Nunnenkamp, A. K. Feofanov, and T. J. Kippenberg, Nonreciprocal reconfigurable microwave optomechanical circuit, Nat. Commun. **8**, 604 (2017).

[57] Mingyun Yuan, Vibhor Singh, Yaroslav M. Blanter, and Gary A. Steele, Large cooperativity and microkelvin cooling with a three-dimensional optomechanical cavity, Nat. Commun. **6,** 8491 (2015).

[58] Atsushi Noguchi, Rekishu Yamazaki, Manabu Ataka, Hiroyuki Fujita, Yutaka Tabuchi, Toyofumi Ishikawa, Koji Usami, and Yasunobu Nakamura, Ground state cooling of a quantum electromechanical system with a silicon nitride membrane in a 3D loop-gap cavity, New J. Phys. **18,** 103036 (2016).

[59] Y. Tsaturyan, A. Barg, E. S. Polzik, and A. Schliesser, Ultracoherent nanomechanical resonators via soft clamping and dissipation dilution, Nat. Nanotechnol. **12,** 776 (2017).

[60] A. H. Ghadimi, S. A. Fedorov, N. J. Engelsen, M. J. Bereyhi, R. Schilling, D. J. Wilson, and T. J. Kippenberg, Elastic strain engineering for ultralow mechanical dissipation, Science **360,** 764 (2018).

[61] Neville H. Fletcher: *Acoustic Systems in Biology* (Oxford University Press, New York, 1992)

[62] Quirin P. Unterreithmeier, Thomas Faust, and Jörg P. Kotthaus, Damping of Nanomechanical Resonators, Phys. Rev. Lett. **105,** 027205 (2010).

[63] Robert O. Pohl, Xiao Liu, and EunJoo Thompson, Low-temperature thermal conductivity and acoustic attenuation in amorphous solids, Rev. Mod. Phys. **74,** 991 (2002).

[64] Carlton M. Caves, Kip S. Thorne, Ronald W. P. Drever, Vernon D. Sandberg, and Mark Zimmermann, On the measurement of a weak classical force coupled to a quantum-mechanical oscillator. I. Issues of principle, Rev. Mod. Phys. **52,** 341 (1980).

[65] Mark F. Bocko and Roberto Onofrio, On the measurement of a weak classical force coupled to a harmonic oscillator: Experimental progress, Rev. Mod. Phys. **68,** 755 (1996).

[66] J. Moser, J. Güttinger, A. Eichler, M. J. Esplandiu, D. E. Liu, M. I. Dykman, and A. Bachtold, Ultrasensitive force detection with a nanotube mechanical resonator, Nat. Nanotechnol. **8,** 493 (2013).

[67] D. J. Wilson, V. Sudhir, N. Piro, R. Schilling, A. Ghadimi, and T. J. Kippenberg, Measurement-based control of a mechanical oscillator at its thermal decoherence rate, Nature **524,** 325 (2015).

[68] Massimiliano Rossi, David Mason, Junxin Chen, Yeghishe Tsaturyan, and Albert Schliesser, Measurement-based quantum control of mechanical motion, Nature **563,** 53 (2018).

[69] J. D. Teufel, F. Lecocq, and R. W. Simmonds, Overwhelming Thermomechanical Motion with Microwave Radiation Pressure Shot Noise, Phys. Rev. Lett. **116,** 013602 (2016).

[70] Uroš Delić, Manuel Reisenbauer, Kahan Dare, David Grass, Vladan Vuletić, Nikolai Kiesel, and Markus Aspelmeyer, Cooling of a levitated nanoparticle to the motional quantum ground state, Science **367,** 892 (2020).

[71] Felix Tebbenjohanns, Martin Frimmer, Vijay Jain, Dominik Windey, and Lukas Novotny, Motional Sideband Asymmetry of a Nanoparticle Optically Levitated in Free Space, Phys. Rev. Lett. **124,** 013603 (2020).

[72] A. Einstein, B. Podolsky, and N. Rosen, Can quantum-mechanical description of physical reality be considered complete? Phys. Rev. **47,** 777 (1935).

[73] Andreas Kronwald, Florian Marquardt, and Aashish A. Clerk, Arbitrarily large steady-state bosonic squeezing via dissipation, Phys. Rev. A **88,** 063833 (2013).

[74] Ying-Dan Wang and Aashish A. Clerk, Reservoir-Engineered Entanglement in Optomechanical Systems, Phys. Rev. Lett. **110,** 253601 (2013).

[75] Huatang Tan, Gaoxiang Li, and P. Meystre, Dissipation-driven two-mode mechanical squeezed states in optomechanical systems, Phys. Rev. A **87,** 033829 (2013).

[76] Lin Tian, Robust Photon Entanglement via Quantum Interference in Optomechanical Interfaces, Phys. Rev. Lett. **110,** 233602 (2013).

[77] M. J. Woolley and A. A. Clerk, Two-mode squeezed states in cavity optomechanics via engineering of a single reservoir, Phys. Rev. A **89,** 063805 (2014).

[78] J. Li, I. Moaddel Haghighi, N. Malossi, S. Zippilli, and D. Vitali, Generation and detection of large and robust entanglement between two different mechanical resonators in cavity optomechanics, New J. Phys. **17,** 103037 (2015).

[79] Matthew Reagor, Hanhee Paik, Gianluigi Catelani, Luyan Sun, Christopher Axline, Eric Holland, Ioan M. Pop, Nicholas A. Masluk, Teresa Brecht, Luigi Frunzio, Michel H. Devoret, Leonid Glazman, and Robert J. Schoelkopf, Reaching 10 ms single photon lifetimes for superconducting aluminum cavities, Appl. Phys. Lett. **102,** 192604 (2013).

[80] Matthew Reagor, Wolfgang Pfaff, Christopher Axline, Reinier W. Heeres, Nissim Ofek, Katrina Sliwa, Eric Holland, Chen Wang, Jacob Blumoff, Kevin Chou, Michael J. Hatridge, Luigi Frunzio, Michel H. Devoret, Liang Jiang, and Robert J. Schoelkopf, Quantum memory with millisecond coherence in circuit QED, Phys. Rev. B **94,** 014506 (2016).

[81] Mingyun Yuan, Martijn A. Cohen, and Gary A. Steele, Silicon nitride membrane resonators at millikelvin temperatures with quality factors exceeding 10^8, Appl. Phys. Lett. **107,** 263501 (2015).

[82] E. E. Wollman, C. U. Lei, A. J. Weinstein, J. Suh, A. Kronwald, F. Marquardt, A. A. Clerk, and K. C. Schwab, Quantum squeezing of motion in a mechanical resonator, Science **349,** 952 (2015).

[83] J.-M. Pirkkalainen, E. Damskägg, M. Brandt, F. Massel, and M. A. Sillanpää, Squeezing of Quantum Noise of Motion in a Micromechanical Resonator, Phys. Rev. Lett. **115,** 243601 (2015).

[84] F. Lecocq, J. B. Clark, R. W. Simmonds, J. Aumentado, and J. D. Teufel, Quantum Nondemolition Measurement of a Nonclassical State of a Massive Object, Phys. Rev. X **5,** 041037 (2015).

[85] Rong Zhang, Yinan Fang, Yang-Yang Wang, Stefano Chesi, and Ying-Dan Wang, Strong mechanical squeezing in an unresolved-sideband optomechanical system, Phys. Rev. A **99,** 043805 (2019).

[86] Stefano Mancini, David Vitali, and Paolo Tombesi, Optomechanical Cooling of a Macroscopic Oscillator by Homodyne Feedback, Phys. Rev. Lett. **80,** 688 (1998).

[87] P. F. Cohadon, A. Heidmann, and M. Pinard, Cooling of a Mirror by Radiation Pressure, Phys. Rev. Lett. **83,** 3174 (1999).

[88] M. Poggio, C. L. Degen, H. J. Mamin, and D. Rugar, Feedback Cooling of a Cantilever's Fundamental Mode below 5 mK, Phys. Rev. Lett. **99**, 017201 (2007).

[89] Clemens Schäfermeier, Hugo Kerdoncuff, Ulrich B. Hoff, Hao Fu, Alexander Huck, Jan Bilek, Glen I. Harris, Warwick P. Bowen, Tobias Gehring, and Ulrik L. Andersen, Quantum enhanced feedback cooling of a mechanical oscillator using nonclassical light, Nat. Commun. **7**, 13628 (2016).

[90] C. Macklin, K. O'Brien, D. Hover, M. E. Schwartz, V. Bolkhovsky, X. Zhang, W. D. Oliver, and I. Siddiqi, A near-quantum-limited Josephson traveling-wave parametric amplifier, Science **350**, 307 (2015).

[91] C. Genes, D. Vitali, P. Tombesi, S. Gigan, and Markus Aspelmeyer, Ground-state cooling of a micromechanical oscillator: Comparing cold damping and cavity-assisted cooling schemes, Phys. Rev. A **77**, 033804 (2008).

[92] Stefano Mancini, David Vitali, and Paolo Tombesi, Motional squashed states, J. Opt. B: Quantum Semiclassical Opt. **2**, 190 (2000).

[93] David Vitali, Stefano Mancini, Luciano Ribichini, and Paolo Tombesi, Mirror quiescence and high-sensitivity position measurements with feedback, Phys. Rev. A **65**, 063803 (2002).

[94] A. Szorkovszky, A. C. Doherty, G. I. Harris, and W. P. Bowen, Mechanical Squeezing via Parametric Amplification and Weak Measurement, Phys. Rev. Lett. **107**, 213603 (2011).

[95] A. Vinante and P. Falferi, Feedback-Enhanced Parametric Squeezing of Mechanical Motion, Phys. Rev. Lett. **111**, 207203 (2013).

[96] M. R. Vanner, I. Pikovski, G. D. Cole, M. S. Kim, Č. Brukner, K. Hammerer, G. J. Milburn, and M. Aspelmeyer, Pulsed quantum optomechanics, Proc. Natl. Acad. Sci. **108**, 16182 (2011).

[97] J. Clarke, P. Sahium, K. E. Khosla, I. Pikovski, M. S. Kim, and M. R. Vanner, Generating mechanical and optomechanical entanglement via pulsed interaction and measurement, New J. Phys. **22**, 063001 (2020).

[98] M. R. Vanner, J. Hofer, G. D. Cole, and M. Aspelmeyer, Cooling-by-measurement and mechanical state tomography via pulsed optomechanics, Nat. Commun. **4**, 2295 (2013).

[99] Juha T. Muhonen, Giada R. La Gala, Rick Leijssen, and Ewold Verhagen, State Preparation and Tomography of a Nanomechanical Resonator with Fast Light Pulses, Phys. Rev. Lett. **123**, 113601 (2019).

[100] Vladimir B. Braginsky, Yuri I. Vorontsov, and Kip S. Thorne, Quantum nondemolition measurements, Science **209**, 547 (1980).

[101] Matteo Brunelli, Daniel Malz, Albert Schliesser, and Andreas Nunnenkamp, Stroboscopic quantum optomechanics, Phys. Rev. Res. **2**, 023241 (2020).

[102] D. N. Bernal-García, H. Vinck-Posada, and M. J. Woolley, Nonstationary force sensing under dissipative mechanical quantum squeezing, arXiv:2007.13051 (2020).

[103] Alok Tripathi and T. S. Vedavathy, Electromagnetic shielding using superconductors, Appl. Supercond. **2**, 1 (1994).

[104] R. Ackermann et al., in Proceedings of the 10th Marcel Grossmann Meeting on General Relativity (World Scientific, Rio de Janeiro, 2003).

[105] E. Olivieri, J. Billard, M. De Jesus, A. Juillard, and A. Leder, Vibrations on pulse tube based dry dilution refrigerators for low noise measurements, Nucl. Instrum. Methods Phys. Res. **858**, 73 (2017).

[106] Martin de Wit, Gesa Welker, Kier Heeck, Frank M. Buters, Hedwig J. Eerkens, Gert Koning, Harmen van der Meer, Dirk Bouwmeester, and Tjerk H. Oosterkamp, Vibration isolation with high thermal conductance for a cryogen-free dilution refrigerator, Rev. Sci. Instrum. **90**, 015112 (2019).

[107] A. M. J. den Haan, G. H. C. J. Wijts, F. Galli, O. Usenko, G. J. C. van Baarle, D. J. van der Zalm, and T. H. Oosterkamp, Atomic resolution scanning tunneling microscopy in a cryogen free dilution refrigerator at 15 mk, Rev. Sci. Instrum. **85**, 035112 (2014).

[108] S. K. Lamoreaux, Demonstration of the Casimir Force in the 0.6 to $6\mu m$ Range, Phys. Rev. Lett. **78**, 5 (1997).

[109] Jaroslaw Labaziewicz, Yufei Ge, Paul Antohi, David Leibrandt, Kenneth R. Brown, and Isaac L. Chuang, Suppression of Heating Rates in Cryogenic Surface-Electrode Ion Traps, Phys. Rev. Lett. **100**, 013001 (2008).

[110] A. Vinante, M. Carlesso, A. Bassi, A. Chiasera, S. Varas, P. Falferi, B. Margesin, R. Mezzena, and H. Ulbricht, Narrowing the Parameter Space of Collapse Models with Ultracold Layered Force Sensors, Phys. Rev. Lett. **125**, 100404 (2020).